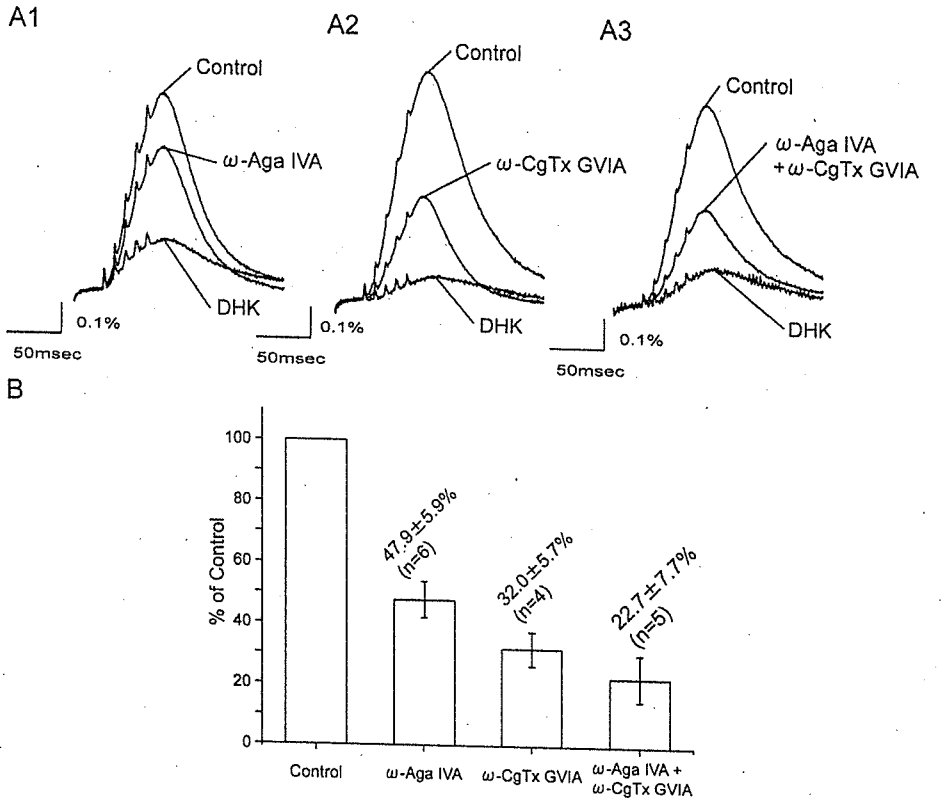

Fig. 5. Effects of Ca^{2+} channel blockers on the amplitude of the synaptically induced glial depolarisation in the presence of an adenosine A_1 receptor blocker. (A) The synaptically induced glial depolarisation was measured in the presence of 8-CPT (10μM), and the blockers for the P/Q-type channel, ω-AgaIVA (1 μM, A1), and/or the N-type channel, ω-CgTxGVIA (1 μM, A2) were applied. Responses were evoked by delivering five stimuli with a 10 ms interval to Schaffer collaterals. The effect of application of ω-CgTxGVIA was greater than that of ω-AgaIVA. Application of DHK (1 mM) suppresses the component due to glutamate uptake, leaving a component which is not related to glutamate release. CNQX(10 μM) and APV(50 μM) were present in the bath in all experiments. (B) Statistical comparison of the effects of Ca^{2+} channel blockers on the synaptically induced glial depolarisation in the presence of 8-CPT (10 μM). After subtracting the DHK-insensitive component, the signal was integrated over the first 200 ms and normalised to the value in control conditions. Each column and bar indicates the mean and S.E.M.

part of the synaptically induced depolarizing signal in the presence of glutamate receptor antagonists could be due to activities of neuronal glutamate transporters because the voltage-sensitive dye we used in this study preferentially stains glial cells but stains neuronal cells as well (Momose-Sato et al., 1999). If it was the case, however, it would not confound our results, because, either way we can monitor amount of glutamate release by measuring the signal that we refer to as synaptically induced glial depolarisation.

There is a possibility that the applied adenosine A_1 receptor agonist and/or antagonist acted on the glial glutamate transporter, rather than on transmitter release. However, application of the adenosine A_1 receptor blocker also facilitated the fEPSPs, implying that the blocker acted on release, not on uptake. To support presynaptic site of drug actions, an immunohistochemical study by Ochiishi et al. (1999) reported that adenosine A_1 receptor immunoreactivity was not detected on glial cells. In addition, it has been reported that glial transporters can be regulated by activation of adenosine A_2 receptors, but not adenosine A_1 receptors (Nishizaki et al., 2002). Thus, it is unlikely that the adenosine A_1 receptor agonist and/or antagonist acted on glial glutamate transporters.

Immunohistochemical studies reported that not only presynaptic but also post synaptic reactivities of adenosine A_1 receptors were detected (Ochiishi et al., 1999, Rebola et al., 2003), and that adenosine A_1 receptors co-localize with postsynaptic NMDA glutamate receptors and N- or P/Q-type voltage-gated Ca^{2+} channels (Rebola et al., 2003). Therefore adenosine A_1 receptor agonist and/or antagonist might have acted on postsynaptic sites. In our experimental condition, however, responses of postsynaptic neurons were blocked by antagonists against ionotropic glutamate receptors. Therefore, signals due to activities of postsynaptic membranes or due to uptake of glutamate from the recurrent terminals of post synaptic neurons were unlikely to be involved in synaptically induced glial depolarisation signal in this study.

It has been shown in previous reports that activation of presynaptic metabotropic glutamate receptors would suppress glutamate release from presynaptic terminals (Cartmell and Schoepp, 2000). To test this possibility, we tested the effects of agonists and antagonists for mGluRs on synaptically induced glial depolarisation signals in normal conditions in which the adenosine A_1 receptor agonist was absent. We found that mGluR agonists suppressed synap-

tically induced glial depolarisation significantly, whereas the antagonists did not significantly enhance synaptically induced glial depolarisation. Although N-type voltage-gated Ca^{2+} channel are the most common voltage-gated Ca^{2+} channels shown to be inhibited by mGluR agonists in literatures (Anwyl, 1999), it is possible that presynaptic mGluRs be more effectively activated in the presence of adenosine A_1 receptor antagonist and the activated mGluRs target P/Q voltage-gated Ca^{2+} channels. We have not tested the effects of mGluR agonists/antagonists in the presence of adenosine A_1 receptor antagonists. Still, we should be able to claim N-type voltage-gated Ca^{2+} channel as the main regulator in normal conditions.

Both in the presence and absence of 8-CPT, the degree of blockade after co-application of ω-AgaIVA and ω-CgTxGVIA was less than the sum of the blockades produced by ω-AgaIVA alone or ω-CgTxGVIA alone. This non-linearity is not surprising, since it has been shown by Reuter (Reuter, 1995) that ω-AgaIVA-sensitive voltage-gated Ca^{2+} channels and ω-CgTxGVIA-sensitive voltage-gated Ca^{2+} channels coexist in more than half of the synaptic terminals of hippocampal cell cultures, and, since the amplitude of the postsynaptic response is likely to be related to the power of the presynaptic Ca^{2+} current (Augustine et al., 1985), the non-linearity may be due to the power relationship between the presynaptic Ca^{2+} current and transmitter release at those terminals in which N- and P/Q-type voltage-gated Ca^{2+} channels coexist. If the tonic suppression of glutamate release mediated by adenosine A_1 receptors is mainly due to inhibition of voltage-gated Ca^{2+} channels, we should be able to estimate the degree of tonic inhibition of N- and P/Q-type voltage-gated Ca^{2+} channels by activation of adenosine A_1 receptors at CA3–CA1 synapses and also the relative contributions of these channels in the absence of inhibition. We assumed that the relationship between the amplitude of the synaptically induced glial depolarisation and the Ca^{2+} rise due to entry through voltage-gated Ca^{2+} channels to be as follows.

Amplitude of the synaptically induced glial depolarisation

$$= constant \times \left(\Delta\left[Ca^{2+}\right]_{pre}\right)^{m}$$

Wu and Saggau (1994b) obtained a value of m=3.5 by analysing their Ca^{2+} imaging data recorded from presynaptic terminals at CA3–CA1 synapses, simultaneously per-

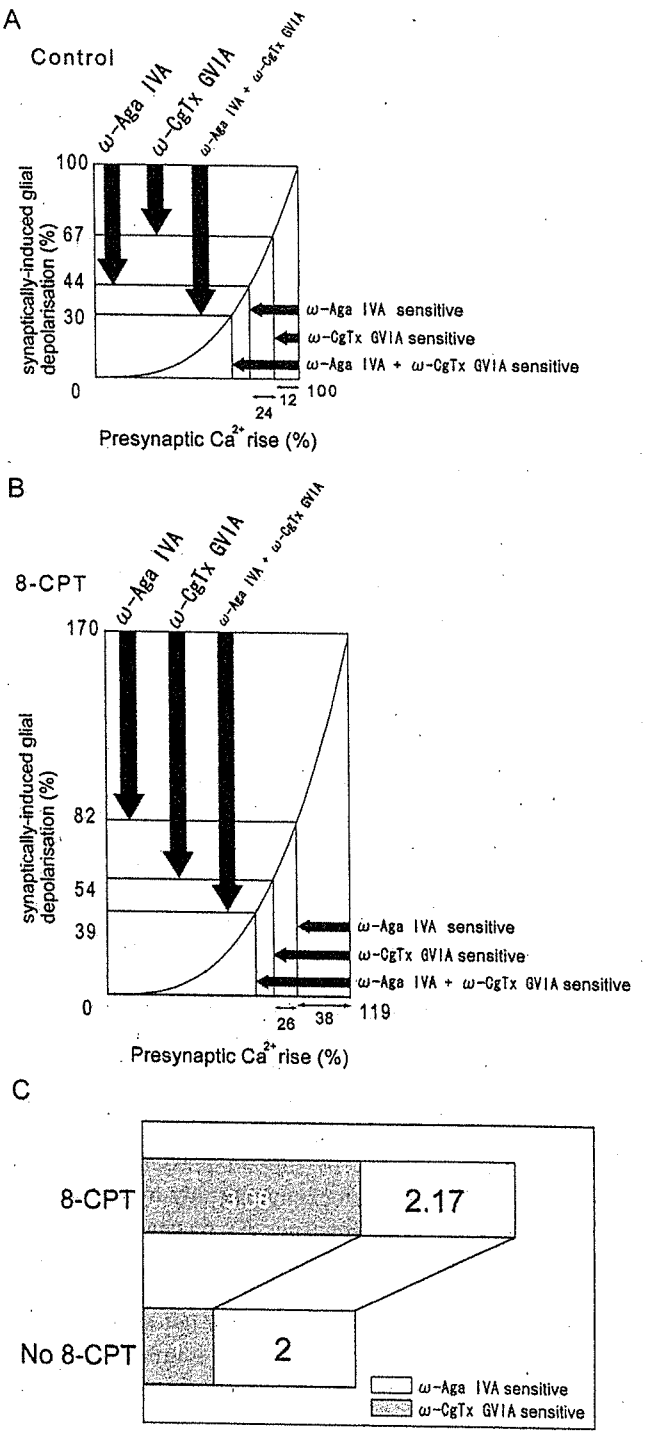

Fig. 6. An analysis of the contribution of voltage-gated Ca^{2+} channels to glutamate release. (A) The relationship between the synaptically induced glial depolarisation and the calculated presynaptic Ca^{2+} influx in the absence of an adenosine A_1 receptor blocker. In this calculation, the amplitude of the synaptically induced glial depolarisation was assumed to be proportional to the third power of the change in the $[Ca^{2+}]_{pre}$; synaptically induced glial depolarisation=constant×$(\Delta[Ca^{2+}]_{pre})^3$. The ordinate shows the relative amplitude of synaptically induced glial depolarisation normalized to the value in the control condition in which 8-CPT was absent. The vertical arrows show the extent of the suppression by blockers for voltage-gated Ca^{2+} channels. The abscissa shows the relative change in calculated presynapitc Ca^{2+} concentration normalized to the value in the control condition. The horizontal arrows show the extent of suppression. (B) The relationship between the synaptically induced glial depolarisation and the calculated presynaptic Ca^{2+} influx in the presence 8-CPT, an adenosine A_1 receptor blocker. The ordinate and the abscissa are normalized to the value obtained in the control condition in which 8-CPT was absent. (C) Comparison of the calculated contribution of voltage-gated Ca^{2+} channels to the change in the $[Ca^{2+}]_{pre}$. The values are normalised to the contribution of the ω-CgTxGVIA-sensitive component in the absence of adenosine A_1 receptor-mediated inhibition.

formed with field EPSP measurements. Reid et al. (1998) estimated m=3.1 or 3.3 at hippocampal autapses. Reid et al. (1998) showed that the values for N- and P/Q-types were not significantly different. Applying this formula, we calculated the relative contribution of different voltage-gated Ca^{2+} channels to the Ca^{2+} rise, based on the effects of the different channel blockers on the synaptically induced glial depolarisation in the absence and in the presence of 8-CPT, the adenosine A_1 receptor blocker. In the absence of 8-CPT, the amplitude of synaptically induced glial depolarisation was reduced by ω-CgTxGVIA alone and ω-AgaIVA alone to 67.4±7.3% and 44.4±6.5% of the control respectively. For m=3, these values correspond to 12% and 24% blockade of the total Ca^{2+} rise (Fig. 6A). In the presence of 10 μM 8-CPT, the amplitude of the synaptically induced glial depolarisation increased to 170% (Fig. 3), corresponding to an increase in the Ca^{2+} rise of 119%. In this condition, the amplitude of synaptically induced glial depolarisation by ω-CgTxGVIA alone and ω-AgaIVA alone was 32.0±5.7% and 47.9±5.9% of control respectively, corresponding to 38% and 26% blockade of the total Ca^{2+} rise in the control conditions with no 8-CPT (Fig. 6B). Thus, the relative contribution of N- and P/Q-type voltage-gated Ca^{2+} channels was 1:2 in the absence of 8-CPT and 3.08:2.17 in the presence of 8-CPT (Fig. 6C). A similar conclusion was reached when we assume m=2, 4 or 5. We can therefore conclude that the N-type voltage-gated Ca^{2+} channel is suppressed by tonic activation of adenosine A_1 receptors, whereas the P-type voltage-gated Ca^{2+} channel is not significantly affected.

Although it has been shown that N- and P/Q-type voltage-gated Ca^{2+} channels are responsible for transmitter release at many synapses in the central nervous systems, the distribution and the contribution of these voltage-gated Ca^{2+} channels seem to vary from synapses to synapses (Reid et al., 1997, 2003; Reuter, 1996). Scholz and Miller (1995) and Iwasaki et al. (2000) also have shown that the relative contribution of N-type versus P/Q-type changes during development. The results of our study suggest a possibility that the extent of adenosine A_1 receptor-mediated tonic inhibition can be one of the reasons for the heterogeneity of voltage-gated Ca^{2+} channels responsible for transmitter release.

The source of adenosine responsible for tonic regulation of synaptic transmission is largely unknown, and we did not make attempts to analyze the source of adenosine in our study. Two possible sources have been suggested: dephosphorylation of ATP released either from presynaptic terminals or glial cells (Newman, 2003; Cunha and Ribeiro, 2000; Dunwiddie and Masino, 2001; Yawo and Chuhma, 1993). Release of adenosine via passive or active transporters is also suggested (Dunwiddie and Masino, 2001). The basal extracellular level of adenosine is reported to be in the range of 25–250 nM. Since the affinity of adenosine A_1 receptors to adenosine is reported to be around 70 nM (Dunwiddie and Masino, 2001), the basal level of adenosine is high enough to provide tonic activation of adenosine A_1 receptors.

Acknowledgements

This work was supported by a grant from the Ministry of Education, Culture, Sports, Science and Technology of Japan (No. 15082207, H.M.).

References

Ambrosio, A.F., Malva, J.O., Carvalho, A.P., Carvalho, C.M., 1997. Inhibition of N-, P/Q- and other types of Ca^{2+} channels in rat hippocampal nerve terminals by the adenosine A1 receptor. Eur. J. Pharmacol. 340, 301–310.

Anwyl, R., 1999. Metabotropic glutamate receptors: electrophysiological properties and role in plasticity. Brain Res. Rev. 29, 83–120.

Augustine, G.J., Charlton, M.P., Smith, S.J., 1985. Ca^{2+} entry into voltage-clamped presynaptic terminals of squid. J. Physiol. 367, 143–162.

Cartmell, J., Schoepp, D.D., 2000. Regulation of neurotransmitter release by metabotropic glutamate receptors. J. Neurochem. 75, 889–907.

Cunha, R.A., Ribeiro, J.A., 2000. ATP as a presynaptic modulator. Life Sci. 68, 119–137.

Dunwiddie, T.V., Masino, S.A., 2001. The role and regulation of adenosine in the central nervous system. Annu. Rev. Neurosci. 24, 31–55.

Iwasaki, S., Momiyama, A., Uchitel, O.D., Takahashi, T., 2000. Developmental changes in Ca^{2+} channel types mediating central synaptic transmission. J. Neurosci. 20, 59–65.

Kawamura, Y., Manita, S., Nakamura, T., Inoue, M., Kudo, Y., Miyakawa, H., 2004. Glutamate release increases during mossy-CA3 LTP but not during Schaffer-CA1 LTP. Eur. J. Neurosci. 19, 1591–1600.

Kim, J.I., Takahashi, M., Ogura, A., Kohno, T., Kudo, Y., Sato, K., 1994. Hydroxyl group of Tyr13 is essential for the activity of omega-conotoxin GVIA, a peptide toxin for N-type Ca^{2+} channel. J. Biol. Chem. 269, 23876–23878.

Kim, J.I., Konishi, S., Iwai, H., Kohno, T., Gouda, H., Shimada, I., Sato, K., Arata, Y., 1995. Three-dimensional solution structure of the Ca^{2+} channel antagonist omega-agatoxin IVA: consensus molecular folding of Ca^{2+} channel blockers. J. Mol. Biol. 250, 659–671.

Kojima, S., Nakamura, T., Nidaira, T., Nakamura, K., Ooashi, N., Ito, E., Watase, K., Tanaka, K., Wada, K., Kudo, Y., Miyakawa, H., 1999. Optical detection of synaptically induced glutamate transport in hippocampal slices. J. Neurosci. 19, 2580–2588.

Luebke, J.I., Dunlap, K., Turner, T.J., 1993. Multiple Ca^{2+} channel types control glutamatergic synaptic transmission in the hippocampus. Neuron 11, 895–902.

Misgeld, U., Bijak, M., Jarolimek, W., 1995. A physiological role for $GABA_B$ receptors and the effects of baclofen in the mammalian central nervous system. Prog. Neurobiol. 46, 423–462.

Mogul, D.J., Adams, M.E., Fox, A.P., 1993. Differential activation of adenosine receptors decreases N-type but potentiates P-type Ca^{2+} current in hippocampal CA3 neurons. Neuron 10, 327–334.

Momose-Sato, Y., Sato, K., Arai, Y., Yazawa, I., Mochida, H., Kamino, K., 1999. Evaluation of voltage-sensitive dyes for long-term recording of neural activity in the hippocampus. J. Membr. Biol. 172, 145–157.

Newman, E.A., 2003. New roles for astrocytes: regulation of synaptic transmission. Trends Neurosci. 26, 536–542.

Nishizaki, T., Nagai, K., Nomura, T., Tada, H., Kanno, T., Tozaki, H., Li, X.X., Kondoh, T., Kodama, N., Takahashi, E., Sakai, N., Tanaka, K., Saito, N., 2002. A new neuromodulatory pathway with a glial contribution mediated via A(2a) adenosine receptors. Glia 39, 133–147.

Ochiishi, T., Saitoh, Y., Yukawa, A., Saji, M., Ren, Y., Shirao, T., Miyamoto, H., Nakata, H., Sekino, Y., 1999. High level of adenosine A_1 receptor-like immunoreactivity in the CA2/CA3a region of the adult rat hippocampus. Neuroscience 93, 955–967.

Rebola, N., Pinheiro, P.C., Oliveira, C.R., Malva, J.O., Cunha, R.A., 2003. Subcellular localization of adenosine A_1 receptors in nerve terminals and synapses of the rat hippocampus. Brain Res. 987, 49–58.

Reid, C.A., Clements, J.D., Bekkers, J.M., 1997. Nonuniform distribution of Ca^{2+} channel subtypes on presynaptic terminals of excitatory synapses in hippocampal cultures. J. Neurosci. 17, 2738–2745.

Reid, C.A., Bekkers, J.M., Clements, J.D., 1998. N- and P/Q type Ca^{2+} channels mediate transmitter release with a similar cooperativity at rat hippocampal autapses. J. Neurosci. 18, 2849–2855.

Reid, C.A., Bekkers, J.M., Clements, J.D., 2003. Presynaptic Ca^{2+} channels: a functional patchwork. Trends Neurosci. 26, 683–687.

Reuter, H., 1995. Measurements of exocytosis from single presynaptic nerve terminals reveal heterogeneous inhibition by Ca^{2+}-channel blockers. Neuron 14, 773–779.

Reuter, H., 1996. Diversity and function of presynaptic Ca^{2+} channels in the brain. Curr. Opin. Neurobiol. 6, 331–337.

Schlicker, E., Kathmann, M., 2001. Modulation of transmitter release via presynaptic cannabinoid receptors. Trends Pharmacol. Sci. 22, 565–572.

Scholz, K.P., Miller, R.J., 1995. Developmental changes in presynaptic Ca^{2+} channels coupled to glutamate release in cultured rat hippocampal neurons. J. Neurosci. 15, 4612–4617.

Takahashi, T., Momiyama, A., 1993. Different types of Ca^{2+} channels mediate central synaptic transmission. Nature 366, 156–158.

Vizi, E.S., 2000. Role of high-affinity receptors and membrane transporters in nonsynaptic communication and drug action in the central nervous system. Pharmacol. Rev., 63–89.

Wheeler, D.B., Randall, A., Tsien, R.W., 1994. Roles of N-type and Q-type Ca^{2+} channels in supporting hippocampal synaptic transmission. Science 264, 107–111.

Wu, L.G., Saggau, P., 1994. Adenosine inhibits evoked synaptic transmission primarily by reducing presynaptic Ca^{2+} influx in area CA1 of hippocampus. Neuron 12, 1139–1148.

Wu, L.G., Saggau, P., 1994. Pharmacological identification of two types of presynaptic voltage-dependent Ca^{2+} channels at CA3–CA1 synapses of the hippocampus. J. Neurosci. 14, 5613–5622.

Wu, L.G., Saggau, P., 1997. Presynaptic inhibition of elicited neurotransmitter release. Trends Neurosci. 20, 204–212.

Yawo, H., Chuhma, N., 1993. Preferential inhibition of ω-conotoxin-sensitive presynaptic Ca^{2+} channels by adenosine autoreceptors. Nature 365, 256–258.

*M. Nakamura**
Y. Ishida
T. Kohno
K. Sato
Y. Oba
H. Nakamura†

Effects of modification at the fifth residue of μ-conotoxin GIIIA with bulky tags on the electrically stimulated contraction of the rat diaphragm

Authors' affiliations:
M. Nakamura, Y. Oba and H. Nakamura, Graduate School of Bioagricultural Sciences, Nagoya University, Chikusa-ku, Nagoya, 464-8601, Japan

Y. Ishida, T. Kohno and K. Sato, Mitsubishi Kagaku Institute of Life Sciences, Machida, Tokyo, 194-8511, Japan

K. Sato, Fukuoka Women's University, Higashi-ku, Fukuoka, 813-8529, Japan

Correspondence to:
M. Nakamura
Department of Applied Physics and Chemistry
The University of Electro-Communications
Chofu
Tokyo
182-8585
Japan
Tel.: 81-424-86-1966
Fax: 81-424-86-1966
E-mail: mnak@pc.uec.ac.jp

*Present address: Department of Applied Physics and Chemistry, The University of Electro-Communications, Chofu, Tokyo, 182-8585, Japan.
†Deceased November 9, 2000.

Dates:
Received 26 November 2003
Revised 3 February 2004
Accepted 30 May 2004

To cite this article:
Nakamura, M., Ishida, Y., Kohno, T., Sato, K., Oba, Y. & Nakamura, H. Effects of modification at the fifth residue of μ-conotoxin GIIIA with bulky tags on the electrically stimulated contraction of the rat diaphragm.
J. Peptide Res., 2004, 64, 110–117.

Key words: avidin; biotin; μ-conotoxin GIIIA; sodium channels; twitch contraction

Abstract: μ-Conotoxin GIIIA, a peptide toxin from the cone snail, blocks muscle-type sodium channels. Thr-5 of μ-conotoxin GIIIA, located on the opposite side of the active site in the globular molecule, was replaced by Cys to which the bulky tags were attached. The tagged μ-conotoxin GIIIA derivatives, except for the phospholipid-tagged one, exerted the biological activity with a potency slightly weaker than natural μ-conotoxin GIIIA. When the biotinylated tags of various lengths were added, the presence of avidin suppressed the action of the biotinylated toxins of <4 nm, but not with 5 nm. The bulky biotinylated tags are useful as a caliper to measure the depth of receptor sites in the channels.

Abbreviations: Biotin20, *N'*-[2-(*N*-Maleimido)ethyl]-*N*-piperazinyl D-biotinamide; Biotin30, 6-{*N'*-[2-(*N*-maleimido)ethyl]-*N*-piperazinylamide}hexyl D-biotinamide; $BM(PEO)_4$, 1,11-bis-maleimidotetraethyleneglycol; Fmoc, 9-fluorenylmethyloxy carbonyl; GIIIA, μ-conotoxin GIIIA; lipid, *N*-[(4-maleimidylmethyl)cyclohexyl-1-carbonyl]-1,2-dihexadecanoyl-*n*-glycero-3-phosphoethanolamine; MALDI-TOF-MS, matrix-assisted laser desorption ionization time-of-flight mass spectrometry; steroid, U-73122.

Introduction

Sodium channels are transmembrane proteins responsible for the voltage-dependent increase in the sodium permeability that initiates action potentials (1). The pore-forming α-subunit of the sodium channels consists of four homologous domains (2). Receptor site I sodium channel toxins such as tetrodotoxin, saxitoxin and μ-conotoxins

block the sodium flux by physically occluding this channel pore (3,4).

μ-Conotoxin GIIIA (GIIIA) is a 22-amino acid peptide toxin isolated from the cone snail *Conus geographus* (Fig. 1) (3,5–8). The three-dimensional structure of GIIIA determined by nuclear magnetic resonance (NMR) (9–11) reveals that this peptide toxin conforms to a discoidal core structure with three intramolecular disulfide bridges and three hydroxyprolines that impart extreme structural rigidity to its backbone. Using μ-conotoxin, the functional roles of numerous pore residues have been elucidated (12–16). The most critical toxin–channel interaction pair identified to date is between Arg-13 of GIIIA and Glu-758 in domain II of the sodium channels (the rat skeletal muscle isoform numbering) with interactions of which about half was electrostatic and half non-electrostatic (12). Furthermore, using μ-conotoxin, the clockwise arrangement of the four internal domains of the sodium channel was revealed (17,18).

Recently, we modified a single amino acid of GIIIA to obtain ligands that are useful for studying the structure–activity relationships of GIIIA (19,20). The Arg-13 modification of GIIIA suggested that both the chemical nature of the guanidium group and its precise position within the pore are important for the activity of GIIIA (20). In contrast, replacing Thr-5 with Ala did not affect the activity of GIIIA (11), as the peptide segment between Cys-4 and Cys-10 faces an opposite side from the active site. Thus, we replaced Thr-5 with Cys to create the toxin derivative [Cys^5]GIIIA, whose free thiol group enables the addition of various chemical groups (19). The three-dimensional structure of [Cys^5]GIIIA was confirmed by circular dichroism (CD) and NMR spectra, and the free SH position of [Cys^5]GIIIA was confirmed by the mass spectrometric method (19). The addition of small tags only modestly affected the biological activity when compared with that of natural GIIIA (19). In this study, our objective is to show that by using bulky tags, the relatively extensive decoration

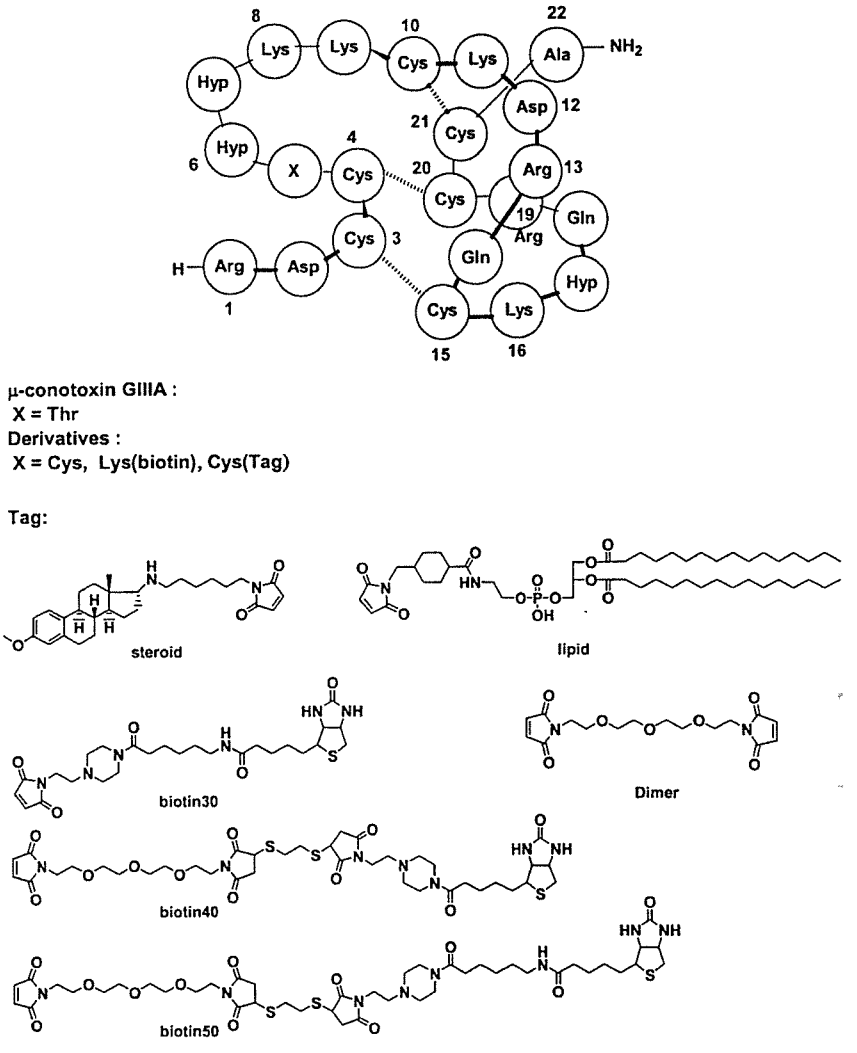

Figure 1. The structure of μ-conotoxin GIIIA (upper) and various tags introduced at the Thr-5 position (bottom). The numbers indicate the amino acid order from the N-terminal.

at the fifth residue of GIIIA could be made without any loss in biological activity. We further investigated the effects of avidin on the biological action of GIIIA tagged with biotinylated long polyether spacers to somehow determine the size of the sodium channel vestibule.

Experimental Procedures

Materials

The 9-fluorenylmethyloxy carbonyl (Fmoc) amino acids, Fmoc-amide resin, and other reagents used for the synthesizer were purchased from Perkin-Elmer–Applied Biosystems (Tokyo, Japan). The other purchased agents were Fmoc-Cys(MeBzl)-OH, and Fmoc-Lys(biotin)-OH (Watanabe Chemicals, Ltd, Hiroshima, Japan); 1,11-bis-maleimidotetraethyleneglycol [BM(PEO)$_4$] (Pierce Chemical Company, Rockford, IL, USA); U-73122 (steroid), avidin (from egg-white) and ethanedithiol (Wako Pure Chemicals, Ltd, Osaka, Japan); *N*-[(4-maleimidylmethyl)cyclohexane-1-carbonyl]-1,2-dihexadecanoyl-*sn*-glycero-3-phosphoethanolamine, triethylammonium salt (lipid) (Molecular Probes, Inc., Eugene, OR, USA); *N'*-[2-(*N*-maleimio)ethyl]-*N*-piperazinyl D-biotinamide, hydrochloride (biotin20) and 6-[*N'*-[2-(*N*-maleimio)ethyl]-*N*-piperazinylamide]hexyl D-biotinamide, hydrochloride (biotin30) (Dojindo Laboratories, Kumamoto, Japan).

Synthesis and purification of peptides

Solid-phase peptide synthesis was performed on a 433A peptide synthesizer (Perkin-Elmer, Applied Biosystems). Matrix-assisted laser desorption ionization time-of-flight mass spectrometry (MALDI-TOF-MS) was measured on a Voyager Linear DE mass spectrometer (PerSeptive Biosystems, Tokyo, Japan) and a Voyager DE Pro mass spectrometer (PerSeptive Biosystems) with α-cyano-4-hydroxycinnamic acid as the matrix. Analytical reverse phase (RP)-high-performance liquid chromatography (HPLC) was conducted on a Shimadzu LC-6 A system (Shimadzu, Kyoto, Japan) with an ODS column Shim-Pack CLC™-ODS (4.6 × 250 mm; Shimadzu) and on a JASCO 1500 system (JASCO, Tokyo, Japan) with an ODS column Develosil ODS-HG-5 (4.6 × 250 mm; Nomura Chemicals, Aichi, Japan). Preparative RP-HPLC was performed on a Shimadzu LC-8 A system (Shimadzu) with an ODS column Shim-Pack PREP-ODS (H) (20 × 250 mm, Shimadzu) and on a JASCO 1500 system (JASCO) with an ODS column Develosil ODS-5 (20 × 250 mm; Nomura Chemicals).

The synthetic method for [Cys^5]GIIIA was previously described (19), and [Lys(biotin)^5]GIIIA was synthesized by a similar procedure. Briefly, linear precursors of the GIIIA derivatives were synthesized by solid phase methodology using Fmoc chemistry. Fmoc-Lys(biotin)-OH was coupled at the fifth position. After trifluoroacetic acid cleavage, the crude linear peptide was diluted to the final peptide concentration of 0.5 mM and subjected to oxidative disulfide bond formation in 0.2 M ammonium acetate buffer (pH 7.8) for 1 day. The crude cyclic products were purified by successive chromatographies on Sephadex G-50F (Amersham Pharmacia Biotech, Uppsala, Sweden), CM-cellulose CM-52 (Whatman International, Ltd, Kent, UK) and preparative RP-HPLC. The major product was purified until it migrated as a single peak during analytical RP-HPLC analysis. The synthetic peptides were analyzed by analytical RP-HPLC and MALDI-TOF-MS measurements.

Syntheses of GIIIA derivatives with steroid and lipid

The maleimide compounds were dissolved at an 8 mM concentration in 0.02 M NH_4OAc (pH 4.0) containing an appropriate amount of acetonitrile or ethanol. To this solution (750 μL, 20 eq) [Cys^5]GIIIA (0.3 μmol) was added in 0.02 M NH_4OAc at pH 4.0 (250 μL), and incubated at room temperature for 20 min. The GIIIA derivatives were purified by analytical RP-HPLC and lyophilized, then analyzed by MALDI-TOF-MS and analytical RP-HPLC.

Synthesis of [Cys(biotin30)^5]GIIIA

For the synthesis of [Cys(biotin30)^5]GIIIA, biotin30 (6 μmol, 20 eq) and [Cys^5]GIIIA (0.3 μmol) were mixed in 0.02 M NH_4OAc at pH 4.0 (1500 μL) then incubated at room temperature for 20 min. [Cys(biotin30)^5]GIIIA was purified by gel filtration using a Sephadex G-25F (1.8 × 28 cm; Amersham Pharmacia Biotech) and analyzed by MALDI-TOF-MS.

Syntheses of [Cys(biotin40)^5]GIIIA and [Cys(biotin50)^5]GIIIA

The synthetic scheme of [Cys(biotin40)^5]GIIIA and [Cys(biotin50)^5]GIIIA is shown in Fig. 2. To a solution of

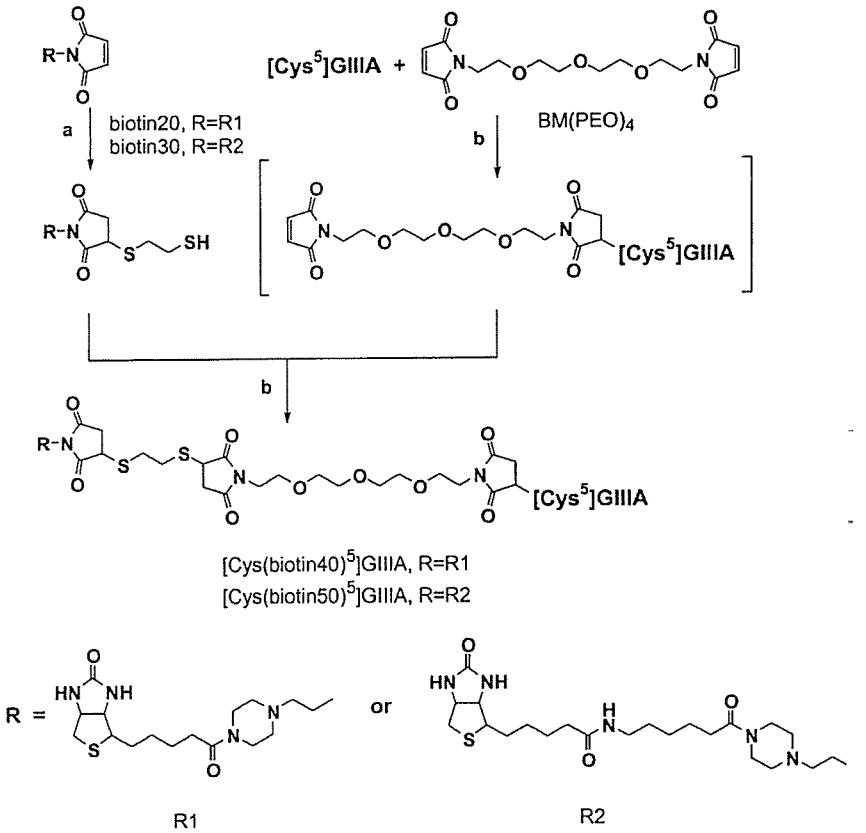

Figure 2. Syntheses of [Cys(biotin40)^5]GIIIA and [Cys(biotin50)^5]GIIIA. The reaction conditions are as follows: (A) ethanedithiol, 0.02 M NH_4OAc, pH 4.0; (B) 0.02 M NH_4OAc, pH 4.0.

biotin20 or biotin30 (8.4 μmol) in 0.02 M NH_4OAc at pH 4.0 (1.68 mL) was added ethanedithiol (10 eq) in 0.02 M NH_4OAc at pH 4.0 (50 μL), then stirred for 1 h, washed with diethyl ether, and lyophilized. The biotinylated compounds were purified by preparative RP-HPLC, and analyzed by MALDI-TOF-MS and analytical RP-HPLC.

To a solution of 5 mM $BM(PEO)_4$ (60 μL, 1 eq) in 0.02 M NH_4OAc at pH 4.0 was added [Cys^5]GIIIA (0.3 μmol) in 0.02 M NH_4OAc at pH 4.0 (90 μL), then incubated at room temperature for 10 min. Six micromoles of the biotinylated compound (150 μL, 3 eq) in 0.02 M NH_4OAc at pH 4.0 was added to this solution, and incubated at room temperature for 20 min. The biotinylated GIIIA derivatives were purified by RP-HPLC and analyzed by MALDI-TOF-MS and analytical RP-HPLC.

Avidin complex

The biotinylated GIIIA derivatives (0.1 μmol) in 0.02 M NH_4OAc at pH 6.7 (50 μL) were added to 1 eq of avidin solution, and the mixture was incubated at room temperature for 1 h, then purified by gel filtration with Sephadex G-50F (1.3 × 5.0 cm) using 0.02 M NH_4OAc at pH 6.7.

CD measurements

The CD spectra were measured using a JASCO J-600 spectropolarimeter (JASCO) in H_2O solution (0.01 M sodium phosphate, pH 7.0) at 20 °C with peptide concentrations of 0.05 mM for 190–250 nm and 1 mM for 240–360 nm in a quartz cell of 1 mm path length. The spectra are expressed as molecular ellipticity ([θ]; degree cm^2/dmol).

Bioassay

The inhibitory effects of the synthesized derivatives on the twitch contraction of skeletal muscle to direct electrical stimuli were assayed, as previously reported (11,19–21). From male Wistar rats (body mass 200–300 g), the diaphragm muscle was excised and cut into four stripes, which were electrically stimulated with 5-ms pulses at 0.1 Hz (supramaximal voltage). The twitch–tension responses were isometrically recorded. The activity of the peptides was expressed as percent inhibition of the twitch response. The IC_{50} value is the concentration of peptide necessary for 50% inhibition of the twitch response. Most IC_{50} values are the mean of two sets of experiments.

Results

Syntheses of GIIIA derivatives

The structures of the synthesized GIIIA derivatives are illustrated in Fig. 1. The effects of the replacement of Thr-5 with Cys-5 or Lys(biotin)-5 on the secondary structure were examined using the CD spectra. The CD spectra for [Cys^5]GIIIA [previously reported in (19)] and [Lys(biotin)^5]-GIIIA (Fig. 3) were as comparable with that of natural GIIIA, suggesting that both [Cys^5]GIIIA and [Lys(biotin)^5]GIIIA have a similar secondary structure as that of GIIIA.

Tags of steroid, lipid, another GIIIA, biotin30, biotin40 and biotin50 were introduced into the GIIIA backbone via the Cys-5 residue (Fig. 1). These GIIIA derivatives in addition to [Lys(biotin)^5]GIIIA were characterized by MALDI-TOF-MS (Table 1). The data of MALDI-TOF-MS fit the calculated molecular masses of GIIIA and its derivatives well.

Inhibitory activity of GIIIA derivatives on muscle contraction

The strong electrical stimuli caused a twitch contraction of the isolated rat diaphragm muscle because of activation of the sodium channels. Although the potency of the GIIIA derivatives are evaluated to be slightly weaker when measuring the contractile response of the isolated diaphragm muscle (IC_{50} = 0.1 μM, in the present experiments) than in measuring activities of the composed skeletal muscle-type sodium channels *in vitro* [IC_{50} = 0.05 μM (15)], the obtained structure-activity relationships are similar between *in vivo* and *in vitro* experiments, showing the most important residue as Arg-13 and the other affecting

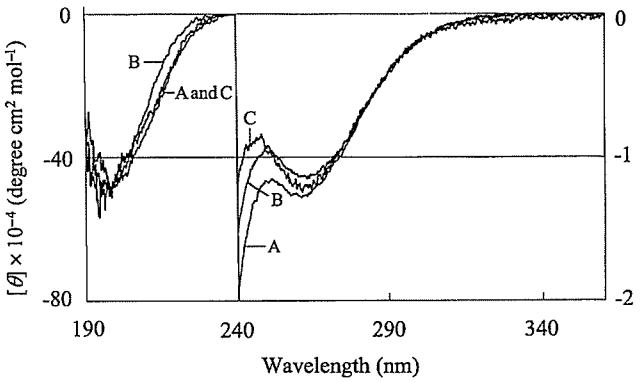

Figure 3. CD spectra of GIIIA (A), [Cys^5]GIIIA (B) and [Lys(biotin)^5]GIIIA (C) in H_2O solution at 20 °C. The vertical axis expresses the molar ellipticity.

residues for the sodium channel inhibition. Thus, the inhibitory effects of the GIIIA derivatives on the twitch contraction have been used as an index of the sodium channel inhibition (11,19–21) and the obtained IC_{50} values (concentrations to inhibit by 50% of twitch contraction) for the tested derivatives are listed in Table 1.

[Cys(steroid)^5]GIIIA was approximately 10 times less potent than natural GIIIA. However, when a lipid functionality was added to [Cys^5]GIIIA, [Cys(lipid)^5]GIIIA did not elicit any inhibitory activity up to 10 μM. In the presence of 10 μM [Cys(lipid)^5]GIIIA, the administration of natural GIIIA inhibited the contraction with normal activity indicating the lack of competition between these peptides (data not shown). With a polyether spacer, [Cys^5]GIIIA was dimerized. The IC_{50} value of the dimeric derivative was only slightly greater than that of natural GIIIA, but the rate of inhibitory response after administration of the dimer was much slower than that of natural GIIIA (data not shown).

[Lys(biotin)^5]GIIIA was approximately six times less potent than natural GIIIA for the inhibition of contraction. However, the inhibitory activity of [Lys(biotin)^5]GIIIA was

Table 1. **Inhibitory activity of skeletal muscle contraction to electric stimulation and MALDI-TOF-MS data of GIIIA and its derivatives**

Compound	MALDI-TOF-MS *m/z* (calc.)	Inhibitory activity IC_{50} (μM)	+ avidin IC_{50} (μM)
GIIIA	2610.4 (2610.0)	0.10	–
[Cys^5]GIIIA	2611.5 (2612.1)	1.9	–
[Cys(steroid)^5]GIIIA	3074.6 (3074.4)	1.3	–
[Cys(lipid)^5]GIIIA	3523.5 (3523.3)	>10	–
Dimer	5575.7 (5575.3)	0.14	–
[Lys(biotin)^5]GIIIA	2862.9 (2863.5)	0.59	>10
[Cys(biotin30)^5]GIIIA	3160.5 (3160.8)	1.00	>3.00
[Cys(biotin40)^5]GIIIA	3493.6 (3494.2)	2.14	>3.00
[Cys(biotin50)^5]GIIIA	3607.8 (3607.4)	1.11	1.64

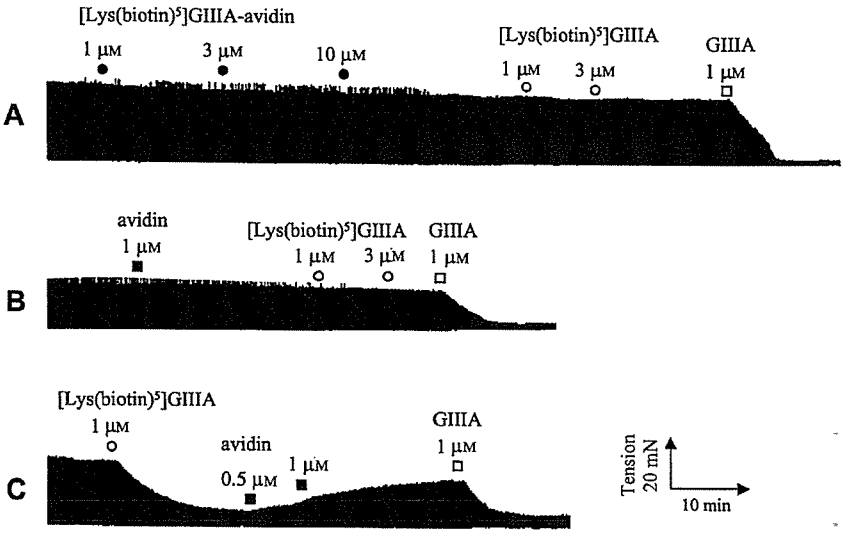

Figure 4. The inhibitory effects of [Lys(biotin)^5]GIIIA and its avidin complex on the contractile response of the isolated rat diaphragm to direct electrical stimuli. (A) [Lys(biotin)^5]GIIIA and then avidin; (B) [Lys(biotin)^5]GIIIA–avidin complex and then [Lys(biotin)^5]GIIIA; (C) GIIIA. Cumulative additions of [Lys(biotin)^5]GIIIA, [Lys(biotin)^5]GIIIA–avidin complex, GIIIA and avidin are indicated by the open circles, closed circles, open squares and closed squares, respectively. The vertical calibration indicates tension (20 mN) and the horizontal one indicates time (10 min).

suppressed in the presence of avidin (Fig. 4). The administration of the preformed [Lys(biotin)^5]GIIIA–avidin complex to the bioassay solution entirely abolished the inhibitory activity of [Lys(biotin)^5]GIIIA.

The inhibitory activities of the [Cys^5]GIIIA derivatives with long spacers between Cys-5 and biotin, [Cys(biotin30)^5]GIIIA, [Cys(biotin40)^5]GIIIA and [Cys(biotin50)^5]-GIIIA, were approximately 10–20 times less potent than that of GIIIA, but were nearly the same as that of [Cys^5]-GIIIA. The administration of avidin in the presence of [Cys(biotin30)^5]GIIIA or [Cys(biotin40)^5]GIIIA suppressed the inhibitory activity in a manner similar to that observed with [Lys(biotin)^5]GIIIA. The preformed avidin complexes of these two derivatives were inactive. The activity loss after the administration of avidin was faster in [Cys(biotin40)^5]GIIIA than in the other biotinylated derivatives. In contrast, the administration of avidin in the presence of [Cys(biotin50)^5]GIIIA did not suppress the inhibitory activity.

Discussion

With respect to the tertiary structure of GIIIA, Thr-5 protrudes from a different face than the biologically active center of Arg-13, and is predicted to point away from the channel vestibule in the toxin-bound channel complex (9–18). In the present experiments, bulky tags composed of various moieties via linkers of different lengths were added to residue 5 of GIIIA, and the tagged-GIIIA derivatives, except for the phospholipid-tagged one, exerted biological activity to various degrees, although the extent of the alteration in the activity of the tagged GIIIA derivatives was rather small when compared to those reported for the modification on Arg-13 of GIIIA (11,12,18,20).

A phospholipid-tagged GIIIA, [Cys(lipid)^5]GIIIA, lost the activity. As the administration of natural GIIIA in the presence of [Cys(lipid)^5]GIIIA elicited an inhibition as under normal conditions, the [Cys(lipid)^5]GIIIA molecule could not reach the binding site in the channel pore. As proposed for the fatty acylation-induced association of SNAP-25, a protein regulating exocytosis, with the membrane (22), [Cys(lipid)^5]GIIIA could be anchored to the lipid component of plasma membrane by the lipid–lipid interaction, and could not reach the binding site in the sodium channel.

Steroid is also hydrophobic to be incorporated into the plasma membrane. However, the steroid-attached GIIIA still elicited the inhibitory activity with the comparable potency with that of [Cys^5]GIIIA. Although we could not interpret this retention of activity well, the hydrophobicity of [Cys(steroid)^5]GIIIA to the lipid component of plasma membrane may be smaller than that of [Cys(lipid)^5]GIIIA, or the affinity of [Cys(steroid)^5]GIIIA to the membrane lipid component may be smaller than that to the receptor site in the channel.

The addition of another GIIIA molecule via a polyether spacer produced a dimer of GIIIA. The inhibitory activity of the dimerized GIIIA was almost the same as that of natural GIIIA, suggesting that this dimer could associate with the receptor in the channel vestibule (Fig. 5, left).

Biotinylated GIIIA with various lengths (approximately 0.5–5 nm) of spacers between the biotin and the fifth residue of GIIIA elicited an inhibition of contraction with a slightly lower potency (6–20 times less) than that of natural GIIIA. Biotinylation of the side chain itself may not markedly affect the inhibitory activity, as [Lys(biotin)^5]GIIIA was

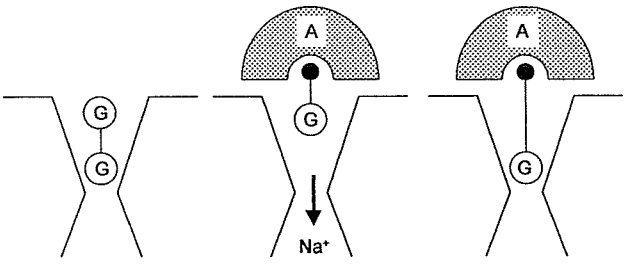

Figure 5. Models of interaction of the dimer (left), biotin analogs with short spacers (center), and with a long spacer (right) with sodium channels. Small black circles, A, and G indicate biotin, avidin, and GIIIA, respectively.

stronger in activity than [Cys^5]GIIIA. Even the biotinylated [Cys^5]GIIIA with the longest side chain tested elicited an inhibitory activity slightly stronger than [Cys^5]GIIIA without a side chain. The presence of non-aliphatic functionalities like a polyester, carbonyl etc. in the side chain may prevent the impedance of the hydrophobic association of the long side chain with the components of the channel vestibule as well as the plasma membrane as postulated for the loss in activity in the case of [Cys(lipid)^5]GIIIA.

In the present experiments, the avidin–biotin interaction affected the biological effects of the biotinylated GIIIA derivatives in a different manner depending on the length of the spacer between the biotin and the fifth residue of GIIIA. The affinity of avidin for biotin is on a fM order (23) that is much stronger than that between GIIIA and the sodium channels being around nM (11,15,24–28). Thus, the presence of avidin abolished the activities of [Lys(biotin)^5]GIIIA, [Cys(biotin30)^5]GIIIA and [Cys(biotin40)^5]GIIIA whose spacer lengths are <4 nm (Fig. 5, center). In contrast, the presence of avidin did not alter the inhibitory action of [Cys(biotin50)^5]GIIIA with the spacer length of 5 nm (Fig. 5, right). The biological activity of these biotinylated analogues should be tested with a concentrated sample. However, a biological assay cannot be run because of a limit to the quantity of the analogues. Although a difference in the IC_{50} value is not seen, the inhibitory activity of the GIIIA analogues with the longer spacer is clearly strong at a lower concentration (the concentration range which does not reach the 50% inhibition). These results suggest that the sodium channel pore structure might have some depth from the entrance to the binding site of GIIIA, as avidin with a large molecular mass of 66 000 could not enter the channel vestibule. When the length from the biotin to the active center of Arg-13 in the conjugates of avidin-biotinylated GIIIA is longer than the depth from the outer surface to the binding site in the channel, the inhibitory effect of the biotinylated GIIIA is not affected by the presence of avidin, otherwise inhibited. When the spacer with the prescribed length is used, the length from the entrance to channel binding sites can be measured, although the length may be linear for the extended configuration but otherwise be curvilinear with the rotation between the C–C bonds or with the interaction between the channel proteins.

The replacement of Thr-5 with Cys enabled the attachment of various tags to the fifth residue of GIIIA. Bulky biotinylated tags with avidin may be useful as a molecular caliper to measure the depth of the binding sites. Previously, we reported that the [Cys^5]GIIIA derivatives with relatively small tags including fluorescence moieties also showed an inhibitory action on muscle contraction (19). Furthermore, we recently succeeded in generating the antibody against μ-conotoxin by i.v. injection of a conjugate of bovine serum albumin-maleimide and [Cys^5]GIIIA, as the conjugate lost its lethal effect on mice as well as its inhibitory activity on muscle (29). Thus, the decoration of a specific residue remote from the active center of peptide toxins may provide a new strategy for the investigation of their association with a receptor as well as for other applications in biological sciences.

Acknowledgments: The authors thank Drs Chikara Sato at the Electrotechnical Laboratory (ETL) and Ronald A. Li at the Johns Hopkins University School of Medicine for their helpful discussions, and Dr Makoto Ojika at Nagoya University for critical reading of the manuscript. This work was partly supported by a grant from CREST, the Japan Science and Technology Corporation and by a Grant-in-Aid for Scientific Research from the Ministry of Education, Science, Sports and Culture of Japan.

References

1. Catterall, W.A. (1998) Structure and function of voltage-sensitive ion channels. *Science* 242, 50–61.
2. Catterall, W.A. (2000) From ionic currents to molecular mechanisms: the structure and function of voltage-gated sodium channels *Neuron* 26, 13–25.
3. Cruz, L.J., Gray, W.R., Olivera, B.M., Zeikus, R.D., Kerr, L., Yoshikami, D. & Moczydlowski, E. (1985) *Conus geographus* toxins that discriminate between neuronal and skeletal muscle sodium channels. *J. Biol. Chem.* 260, 9280–9285.
4. Cestèle, S. & Catterall, W.A. (2000) Molecular mechanisms of neurotoxin action on voltage-gated sodium channel. *Biochimie* 82, 883–892.

5. Nakamura, H., Kobayashi, J., Ohizumi, Y. & Hirata, Y. (1983) Isolation and amino acid compositions of geographutoxin I and II from the marine snail *Conus geographus* Linne. *Experientia* **39**, 590–591.
6. Stone, B.L. & Gray, W.R. (1982) Occurrence of hydroxyproline in a toxin from the marine snail *Conus geographus*. *Arch. Biochem. Biophys.* **216**, 765–767.
7. Sato, S., Nakamura, H., Ohizumi, Y., Kobayashi, J. & Hirata, Y. (1983) The amino acid sequences of homologous hydroxyproline containing myotoxins from the marine snail *Conus geographus* venom. *FEBS Lett.* **155**, 277–280.
8. Gray, W.R. & Olivera, B.M. (1988) Peptide toxins from venomous *Conus* snails. *Ann. Rev. Biochem.* **57**, 665–700.
9. Lancelin, J.-M., Kohda, D., Tate, S.-I., Yanagawa, Y., Abe, T., Satake, M. & Inagaki, F. (1991) Tertiary structure of conotoxin GIIIA in aqueous solution. *Biochemistry* **30**, 6908–6916.
10. Wakamatsu, K., Kohda, D., Hatanaka, H., Lancelin, J.-M., Ishida, Y., Oya, M., Nakamura, H., Inagaki, F. & Sato, K. (1992) Structure–activity relationships of μ-conotoxin GIIIA: structure determination of active and inactive sodium channel blocker peptide by NMR and simulated annealing calculations. *Biochemistry* **31**, 12577–12584.
11. Sato, K., Ishida, Y., Wakamatsu, K., Kato, R., Honda, H., Ohizumi, Y., Nakamura, H., Ohya, M., Lancelin, J.-M., Kohda, D. & Inagaki, F. (1991) Active site of μ-conotoxin GIIIA, a peptide blocker of muscle sodium channels. *J. Biol. Chem.* **266**, 16989–16991.
12. Chang, N.S., French, R.J., Lipkind, G.M., Fozzard, H.A. & Dudley S.C. Jr (1998) Predominant interactions between μ-conotoxin Arg-13 and the skeletal muscle Na^+ channel localized by mutant cycle analysis. *Biochemistry* **37**, 4407–4419.
13. Lipkind, G.M. & Fozzard, H.A. (2000) KcsA crystal structure as framework for a molecular model of the Na^+ channel pore. *Biochemistry* **39**, 8161–8170.
14. Escobar, L., Root, M.J. & MacKinnon, R. (1993) Influence of protein surface change on the bimolecular kinetics of a potassium channel peptide inhibitor. *Biochemistry* **32**, 6982–6987.
15. Chahine, M., Chen, L.-Q., Fotouhi, N., Walsky, R., Fry, D., Santarelli, V., Horn, R. & Kallen, R.G. (1995) Characterizing the μ-conotoxin binding site on voltage-sensitive sodium channels with toxin analogs and channel mutations. *Recept. Channels* **3**, 161–174.
16. Li, R.A., Ennis, I.L., Vélez, P., Tomaselli, G.F. & Marbán, E. (2000) Novel structural determinants of μ-conotoxin (GIIIB) block in rat skeletal muscle (μ1) Na^+ channels. *J. Biol. Chem.* **275**, 27551–27558.
17. Li, R.A., Ennis, I.L., French, R.J., Dudley S.C. Jr, Tomaselli, G.F. & Marbán, E. (2001) Clockwise domain arrangement of the sodium channel revealed by μ-conotoxin (GIIIA) docking orientation. *J. Biol. Chem.* **276**, 11072–11077.
18. Dudley S.C.Jr, Chang, N., Hall, J., Lipkind, G., Fozzard, H.A. & French, R.J. (2000) μ-Conotoxin GIIIA interactions with the voltage-gated Na^+ channel predict a clockwise arrangement of the domains. *J. Gen. Physiol.* **116**, 679–689.
19. Nakamura, M., Ishida, Y., Kohno, T., Sato, K. & Nakamura, H. (2001) Synthesis of [Cys^5]μ-conotoxin GIIIA and its derivatives as a probe of Na^+ channel analysis. *Biochem. Biophys. Res. Commun.* **283**, 374–378.
20. Nakamura, M., Niwa, Y., Ishida, Y., Kohno, T., Sato, K., Oba, Y. & Nakamura, H. (2001) Modification of Arg-13 of μ-conotoxin GIIIA with piperidinyl-Arg analogs and their relation to the inhibition of sodium channels. *FEBS Lett.* **503**, 107–110.
21. Spence, I., Gillessen, D., Gregson, R.P. & Quinn, R.J. (1978) Characterization of the neurotoxic constituents of *Conus geographus* (L) venom. *Life Sci.* **21**, 1759–1770.
22. Hess, D.H., Slater, T.M., Wilson, M.C. & Skene, J.H. (1992) The 25 kDa synaptosomal-associated protein SNAP-25 is the major methionine-rich polypeptide in rapid axonal transport and a major substrate for palmitoylation in adult CNS. *J. Neurosci.* **12**, 4634–4641.
23. Green, N.M. (1990) Avidin and streptavidin. *Methods Enzymol.* **184**, 51–67.
24. Moczydlowski, E., Olivera, B.M., Gray, W.R. & Strichartz, G.R. (1986) Discrimination of muscle and neuronal Na-channel subtypes by binding competition between [^{3}H] saxitoxin and μ-conotoxins. *Proc. Natl Acad. Sci. USA* **83**, 5321–5325.
25. Becker, S., Prusak-Sochaczewski, E., Zamponi, G., Beck-Sickinger, A.G., Gordon, R.D. & French, R.J. (1992) Action of derivatives of μ-conotoxin GIIIA on sodium channels. Single amino acid substitutions in the toxin separately affect association and dissociation rates. *Biochemistry* **31**, 8229–8238.
26. Chen, L.-Q., Chahine, M., Kallen, R.G., Barchi, R.L. & Horn, R. (1992) Chimeric study of sodium channels from rat skeletal and cardiac muscle. *FEBS Lett.* **309**, 253–257.
27. Stephan, M.M., Potts, J.F. & Angue, W.S. (1994) The μ1 skeletal muscle sodium channel: mutation E403Q eliminates sensitivity to tetrodotoxin but not to μ-conotoxins GIIIA and GIIIB. *J. Membr. Biol.* **137**, 1–8.
28. Dudley S.C. Jr, Todt, H., Lipkind, G. & Fozzard, H.A. (1995) A μ-conotoxin-insensitive Na^+ channel mutant: implications for the structure of the outer vestibule. *Biophys. J.* **69**, 1657–1665.
29. Nakamura, M., Oba, Y., Mori, T., Sato, K., Ishida, Y., Matsuda, T. & Nakamura, H. (2002) Generation of polyclonal antibody against μ-conotoxin GIIIA using an immunogen of [Cys^5]μ-conotoxin GIIIA site-specifically conjugated with bovine serum albumin. *Biochem. Biophys. Res. Commun.* **290**, 1037–1041.

JOURNAL OF VIROLOGY, Jan. 2005, p. 214–224
0022-538X/05/$08.00+0 doi:10.1128/JVI.79.1.214–224.2005

Vol. 79, No. 1

Unrestricted Hepatocyte Transduction with Adeno-Associated Virus Serotype 8 Vectors in Mice

Hiroyuki Nakai,[1]* Sally Fuess,[1] Theresa A. Storm,[1] Shin-ichi Muramatsu,[2] Yuko Nara,[2] and Mark A. Kay[1,3]

Departments of Pediatrics[1] and Genetics,[3] Stanford University School of Medicine, Stanford, California, and Neurology, Department of Medicine, Jichi Medical School, Minamikawachi, Tochigi, Japan[2]

Received 18 May 2004/Accepted 20 August 2004

Recombinant adeno-associated virus (rAAV) vectors can mediate long-term stable transduction in various target tissues. However, with rAAV serotype 2 (rAAV2) vectors, liver transduction is confined to only a small portion of hepatocytes even after administration of extremely high vector doses. In order to investigate whether rAAV vectors of other serotypes exhibit similar restricted liver transduction, we performed a dose-response study by injecting mice with β-galactosidase-expressing rAAV1 and rAAV8 vectors via the portal vein. The rAAV1 vector showed a blunted dose-response similar to that of rAAV2 at high doses, while the rAAV8 vector dose-response remained unchanged at any dose and ultimately could transduce all the hepatocytes at a dose of 7.2×10^{12} vector genomes/mouse without toxicity. This indicates that all hepatocytes have the ability to process incoming single-stranded vector genomes into duplex DNA. A single tail vein injection of the rAAV8 vector was as efficient as portal vein injection at any dose. In addition, intravascular administration of the rAAV8 vector at a high dose transduced all the skeletal muscles throughout the body, including the diaphragm, the entire cardiac muscle, and substantial numbers of cells in the pancreas, smooth muscles, and brain. Thus, rAAV8 is a robust vector for gene transfer to the liver and provides a promising research tool for delivering genes to various target organs. In addition, the rAAV8 vector may offer a potential therapeutic agent for various diseases affecting nonhepatic tissues, but great caution is required for vector spillover and tight control of tissue-specific gene expression.

Liver-directed gene transfer with viral and nonviral vectors has been explored for the treatment of a variety of inherited and acquired diseases, including hemophilia (51), various metabolic diseases such as mucopolysaccharidosis (42), hyperlipidemia (24), tyrosinemia (41), and diabetes mellitus (25), and chronic viral hepatitis (29). Among the vectors used to deliver genes to hepatocytes in vivo, recombinant adeno-associated virus (rAAV) vectors are one of the most promising vehicles because they are based on nonpathogenic viruses, transduce both dividing and nondividing cells, and achieve long-term stable transgene expression with minimal toxicity and cellular immune response in animals.

AAV is a small, nonpathogenic, replication-defective parvovirus with a single-stranded DNA genome. Among the various serotypes of AAV, rAAV vectors based on AAV serotype 2 (rAAV2) have been most extensively investigated as gene delivery vectors in vivo, demonstrating efficacy and safety. Based on successful results in a series of preclinical studies for rAAV2-mediated gene therapy, several clinical trials were initiated for the treatment of inherited diseases, including hemophilia B (22).

Despite such recent advances, rAAV2-mediated hepatic gene transfer has still been suboptimal and transduction efficiency in the liver remains unsatisfactory, particularly in cases that require higher transduction efficiency. One major drawback in this system is that only ≈10% of hepatocytes are stably transducible with rAAV2 vectors (5, 39, 59). In other words, it is not possible to increase transduction efficiency in mice (either number of transduced hepatocytes or expression of transgene products) in proportion to given doses when vector doses of 3.0×10^{11} vector genomes (vg) or more are administered per mouse. Liver transduction becomes saturated at higher doses, with transduction efficiencies of around 10% of total hepatocytes (39). The mechanism of this restricted liver transduction has not been elucidated but is not related to impaired uptake of vector particles by hepatocytes because rAAV2 vector genomes are found in a majority of hepatocytes within 24 h after vector infusion (32). We have reasoned from our observations that, in the liver, there are two distinct hepatocyte subpopulations with different metabolic states. That is, only a small subset of hepatocytes have all the machinery required for establishing stable rAAV2 transduction, while the other subset is devoid of some machinery for the process or has some inhibitory machinery that prevents the process (32). Recently, Thomas et al. proposed a model in which the rate of capsid uncoating determines the transduction efficiency with rAAV vectors in the liver (54).

In the past 5 years, there have been several major breakthroughs in rAAV vector technologies that include productions of rAAV vectors derived from alternative serotypes (6, 7, 15, 17, 46, 47, 60) and the development of self-complementary (or double-stranded) rAAV vectors (13, 30, 31, 57). Over a hundred different AAV sequences have been isolated thus far from human and nonhuman primates (14). Their recombinants have been investigated extensively for tissue tropism and transduction efficiency, enabling a dramatic increase in transduction

* Corresponding author. Mailing address: Department of Pediatrics, Stanford University School of Medicine, 300 Pasteur Dr., Grant Bldg., Rm. S374, Stanford, CA 94305. Phone: (650) 498-2753. (650) 725-7487. Fax: (650) 736-2068. E-mail: nakaih@stanford.edu.

efficiency (4, 14, 15) and a change of tissue or cell type tropism or vector distribution patterns in a given tissue (7, 53, 56). Now, finding the optimal AAV serotypes for efficient and tissue-specific transduction has become imperative for successful gene therapy. The other breakthrough, packaging of double-stranded vector genomes into virions, i.e., self-complementary rAAV, has greatly enhanced transduction efficiency, although the vectors can only hold half of the genome.

We and others have established a method by which rAAV2 vector genomes can be cross-packaged into heterologous capsid proteins derived from alternative serotypes, making chimeric virions, so-called pseudo-serotyped rAAV vectors (17, 46). This allowed us to conduct a thorough side-by-side study to compare liver transduction efficiency among different pseudo-serotyped rAAV vectors, types 1 to 6, in mice. Although the rAAV1, -2, and -6 vectors achieved similar expression levels and none of the other serotypes resulted in a dramatic increase in stable liver transduction efficiency (17), the rAAV1, -2, and -6 vectors each exhibited distinct dose-response profiles (17). We have established in two independent studies that rAAV2-mediated stable liver transduction is proportional to given vector doses ranging from 2 to 4×10^9 to 3 to 4×10^{11} vg/mouse (17, 39). Interestingly, and unlike the rAAV2 vector, rAAV1 vector administration into the liver resulted in a disproportionately greater increase in stable liver transduction, as vector doses increased within the same dose range (17), although this dose-response profile for rAAV1 was blunted at doses higher than 4×10^{11} vg/mouse. Since we quantified the transgene product and not the number of transduced hepatocytes in the previous study, it is not known if rAAV1-mediated liver transduction is also confined to a small population of hepatocytes.

In the present study, we investigated whether restricted liver transduction is also the case for pseudo-serotyped rAAV1 and rAAV8 vectors. The rAAV1 vector was selected because it exhibited a distinct dose-response profile, while the rAAV8 vector was chosen because it has been shown to transduce mouse hepatocytes better than rAAV2 (15, 49, 54). As a result, in contrast to rAAV2 vectors, we find that all the hepatocytes are permissive to stable rAAV8 transduction and ≈100% hepatocyte transduction is achievable by portal vein injection at a dose of 7.2×10^{12} vg/mouse. In addition, and unlike the situation with rAAV2 vectors, we find that such high transduction efficiency is achievable by a single tail vein injection of rAAV8 vectors. Finally, we elucidate that the rAAV8 vector can transduce skeletal muscle throughout the body, the entire cardiac muscle, and substantial numbers of pancreatic cells, smooth muscle cells, and brain cells after intravenous injection. These observations not only help us understand the mechanisms of rAAV vector transduction but also emphasize both the utility and promiscuity of rAAV8 vectors.

MATERIALS AND METHODS

Construction of rAAV vectors. The construction and production of the rAAV2 vectors AAV2-EF1α-nlslacZ, AAV2-hF.IX16, and AAV2-CMV-lacZ were described elsewhere (23, 37, 39, 40), although we did not clearly denote the serotype in the vector names in our previous publications. Briefly, AAV2-EF1α-nlslacZ is a bacterial β-galactosidase-expressing rAAV2 vector harboring the human elongation factor 1α (EF1α) enhancer-promoter, the *Escherichia coli lacZ* gene with a nuclear localization signal (nls), and the simian virus 40 poly(A) signal. AAV2-hF.IX16 is a human coagulation factor IX (hF.IX)-expressing rAAV2 vector comprising a liver-specific promoter (the apolipoprotein E hepatic locus control region-human α1-antitrypsin gene promoter) (32), hF.IX minigene (containing a 1.4-kb DNA fragment of the first intron from the hF.IX gene), and the bovine growth hormone poly(A) signal. AAV2-CMV-lacZ is a β-galactosidase-expressing rAAV2 vector harboring the human cytomegalovirus enhancer-promoter with an intron from the human growth hormone gene, the cytosolic *lacZ* gene, and the simian virus 40 poly(A) signal.

For AAV1-EF1α-nlslacZ, AAV8-EF1α-nlslacZ, and AAV8-CMV-lacZ, rAAV2 vector genomes were cross-packaged into capsids derived from AAV serotype 1 or 8 with the corresponding AAV helper plasmids (15, 17) (the AAV8 helper plasmid was kindly provided by James M. Wilson). All the vectors were produced by the triple transfection method, purified by two cycles of cesium chloride gradient centrifugation, and concentrated as outlined elsewhere (3, 17). The final viral preparations were kept in phosphate-buffered saline (PBS) containing 5% sorbitol. The physical particle titers were determined by a quantitative dot blot assay.

Animal procedure. Six- to 8-week-old male C57BL/6 and C57BL/6 *rag-1* mice were purchased from Jackson Laboratory (Bar Harbor, Maine). The portal vein and tail vein injections of rAAV vector preparations were performed as previously described (34, 35). Controls were naïve uninjected mice or mice injected with the excipient (PBS–5% sorbitol) only. Blood samples were periodically collected from the retroorbital plexus. All the animal experiments were performed according to the guidelines for animal care at Stanford University.

Protein analysis. We extracted total liver proteins and determined expression levels of β-galactosidase in rAAV vector-transduced mouse livers with a β-galactosidase enzyme-linked immunosorbent assay kit (Roche Molecular Biochemicals, Indianapolis, Ind.) as previously described (37). We normalized β-galactosidase levels with the total protein concentration determined by the Lowry assay, using a DC protein assay kit (Bio-Rad, Hercules, Calif.), and described the values as picograms of β-galactosidase per milligram of protein. We measured human coagulation factor IX levels in mouse plasma by an enzyme-linked immunosorbent assay specific for human coagulation factor IX. We measured levels of serum alanine aminotransferase (ALT) with the ALT reagent set (Teco Diagnostics, Anaheim, Calif.).

Histological analysis. Pieces of mouse liver lobes were embedded in Tissue-Tek Optimal Cutting Temperature compound (Sakura Finetek USA, Inc., Torrance, Calif.) and frozen on dry ice. In some instances, various mouse tissues other than the liver, i.e., brain, lung, heart, spleen, kidney, intestine, testis, pancreas, and skeletal muscle (quadriceps, tibialis anterior, or tongue), were also collected and processed in the same way. For histochemical detection of β-galactosidase expression, 10-μm sections were cut, fixed with 1.25% glutaraldehyde, stained with 5-bromo-4-chloro-3-indolylphosphate (X-Gal) as described (21), and counterstained with light hematoxylin or nuclear fast red. To determine transduction efficiency in the liver, at least 2,000 nuclei per section were examined for β-galactosidase expression from each animal.

In order to determine cell types in the brain transduced with the rAAV8 vector, we performed immunohistochemical analysis of brain sections. The blocks were cut into coronal sections 12-μm thick with a cryostat. The sections were placed on gelatin-coated slides and dried at room temperature for 30 min. The sections were fixed in 4% paraformaldehyde for 15 min and washed three times in PBS for 5 min. The sections were blocked with PBS containing 5% goat serum at room temperature for 30 min. The sections were incubated with primary antibodies against β-galactosidase (1:200; rabbit immunoglobulin G fraction; Invitrogen, Carlsbad, Calif.), with a mixture of mouse monoclonal anti-NeuN antibody (1:200; Chemicon International Inc.), or mouse monoclonal anti-glial fibrillary acidic protein (GFAP) antibody (1:200; Chemicon International Inc.) in PBS containing 5% goat serum at room temperature for 1 h. NeuN and GFAP served as markers for neurons and astrocytes, respectively. The sections were washed three times in PBS for 5 min. Then they were incubated with Alexa Fluor 488-conjugated goat anti-rabbit immunoglobulin G (2 μg/ml; Invitrogen) and Alexa Fluor 594-conjugated goat anti-mouse immunoglobulin G (2 μg/ml; Invitrogen) in PBS at room temperature for 30 min. The sections were washed three times with PBS for 5 min. Finally, the sections were mounted in Vectashield (Vector Laboratories, Burlingame, Calif.). Immunoreactivity was assessed and viewed under a confocal laser-scanning microscope (TCS NT; Leica).

For detection of pancreatic islet cells, we performed X-Gal and insulin double staining as previously described (55). For detection of Kupffer cells in the liver, we performed X-Gal and F8/40 double staining. Briefly, frozen sections in Optimal Cutting Temperature compound were cut 10-μm thick, air dried for 15 min, and stored at −20°C. Samples were thawed for 1.5 h and then fixed in chilled acetone at −20°C for 20 min. Samples were dried for 6 min and rehydrated in PBS for 10 min. Slides were stained for X-Gal overnight and washed three times in PBS for 5 min. Samples were incubated in 0.3% hydrogen peroxide

TABLE 1. Hepatocyte transduction with AAV1-, AAV2-, or AAV8-EF1α-nlslacZ 6 weeks postinjection

Vector	Dose (vg/mouse)	No. of mice	Mean transduction efficiency (%)[a] ± SD	Mean β-galactosidase expression (pg/mg of protein)[b] ± SD	Mean vector copy no. (ds-vg/dge) ± SD	Mean net vector copy no. per transduced cell (ds-vg/dge)[c] ± SD	Mean β-galactosidase expression rate[d] ± SD	Mean vector genome activity[e] ± SD
AAV1	5.0×10^{10}	4	4.2 ± 1.0	426 ± 110	1.1 ± 0.2	27.0 ± 3.1	100.5 ± 9.5	376.7 ± 67.4
	3.0×10^{11}	6	7.7 ± 0.7	1215 ± 263	9.3 ± 0.9	121.6 ± 14.2	160.1 ± 40.5	133.3 ± 38.4
	1.8×10^{12}	4	13.2 ± 2.5	2078 ± 389	54.9 ± 18.1	413.5 ± 83.1	159.7 ± 27.8	40.1 ± 12.1
	7.2×10^{12}	3	23.5 ± 1.0	2057 ± 99	92.3 ± 12.2	412.1 ± 69.6	88.9 ± 8.0	21.5 ± 1.6
AAV2	3.0×10^{11}	6	3.9 ± 0.5	888 ± 228	5.1 ± 2.0	132.2 ± 47.5	235.8 ± 72.4	197.0 ± 92.5
AAV8	5.0×10^{10}	4	8.1 ± 1.8	1669 ± 201	7.2 ± 1.5	90.6 ± 5.3	211.7 ± 31.5	223.5 ± 23.5
	3.0×10^{11}	6	14.9 ± 3.4	2963 ± 517	58.2 ± 10.9	413.1 ± 134.8	208.2 ± 63.5	53.0 ± 14.6
	1.8×10^{12}	3	65.8 ± 9.0	9052 ± 1541	207.5 ± 56.0	318.4 ± 87.5	140.8 ± 40.2	44.8 ± 7.4
	7.2×10^{12}	4	97.4 ± 0.3	21686 ± 3051	620.6 ± 42.8	637.2 ± 42.6	222.7 ± 31.4	35.3 ± 7.2
None (excipient)		3	0.0	<4	0.0	0.0	NA	NA

[a] X-Gal-positive nuclei/total hepatocyte nuclei counted (at least 2,000 hepatocyte nuclei were counted).
[b] β-Galactosidase antigen levels in liver extracts were normalized to the amount of total protein in samples.
[c] Net vector copy number is defined as the number of double-stranded vector genomes per transduced hepatocyte; i.e., (vector copy number per cell [vg/dge]/transduction efficiency [%]) × 100.
[d] β-Galactosidase expression rate is defined as picograms of β-galactosidase protein per milligram of cellular protein produced from transduced hepatocytes corresponding to 1% of total hepatocytes; i.e., β-galactosidase expression divided by transduction efficiency. The values reflect β-galactosidase production per transduced hepatocyte. NA, not applicable.
[e] Vector genome activity is defined as β-galactosidase production per double-stranded vector genome; i.e., β-galactosidase expression divided by vector copy number (ds-vg/dge).

in methanol for 10 min, rinsed in water, and washed again in PBS. Sections were blocked in 10% normal rabbit serum (Vector Laboratories) with avidin (avidin/biotin blocking kit, Vector Laboratories) in PBS–1% bovine serum albumin for 45 min. Slides were blotted and incubated with F4/80 (1:50 dilution; Serotec, Oxford, United Kingdom) with biotin in PBS–1% bovine serum albumin at room temperature for 1 h. Samples were washed in PBS and incubated for 30 min in anti-rat immunoglobulin G (Vector Laboratories) at a 1:500 dilution in PBS–1% bovine serum albumin. Slides were washed in PBS and incubated for 30 min in the Vectastain Elite ABC kit (Vector Laboratories) according to the manufacturer's instructions. Sections were washed in PBS, rinsed in water, and developed with diaminobenzidine with a diaminobenzidine substrate kit (Vector Laboratories) for 2 to 5 min. Slides were then counterstained with hematoxylin, dehydrated, and coversliped.

DNA analysis. We extracted total genomic DNA from each tissue by a standard phenol chloroform method. We performed Southern blot analysis to determine double-stranded vector genome copy number per diploid genomic equivalent (ds-vg/dge) and to analyze vector forms in transduced tissues as previously described (35, 39). Briefly, we digested 10 μg of total genomic DNA with BglI, which cuts the vector genome seven times, and separated the digests on 0.8% agarose gels, transferred the DNA onto nylon membranes, and hybridized the blotted membrane with a 2.1-kb radioactive vector sequence-specific *lacZ* probe (2.1-kb BglI/BglI fragment, nucleotide positions 1518 to 3639 of the 4,828-base AAV2-EF1α-nlslacZ vector genome). We detected and quantified the signals with a Phosphorimager and Quantity One software (*Bio-Rad*). For analysis of the molecular forms of the vector genomes, we digested sample DNA with BamHI, a single cutter that asymmetrically cleaves the 4,828-base vector genome at nucleotide position 1362, or KpnI, which does not cut the vector genome, and probed with the same *lacZ* probe. The double-stranded vector genome copy number standards were prepared by adding an equivalent number of pAAV-EF1α-nlslacZ (37) plasmid molecules to 10 μg of total genomic DNA extracted from naive mouse liver. The net vector copy number per hepatocyte represents the number of double-stranded vector genomes per transduced hepatocyte and is calculated based on a presumption that double-stranded vector genomes in the liver are carried only by transduced hepatocytes (33, 52).

RESULTS

All the hepatocytes were permissive to stable rAAV8 vector transduction. We previously demonstrated that only a small portion of hepatocytes are permissive to stable rAAV2 vector transduction, which restricts a linear vector dose-response at doses higher than 3.0×10^{11} vg/mouse (39). The maximum number of stably transducible hepatocytes may vary depending on the experimental settings, but it normally plateaus at ≈10% of total hepatocytes. In order to investigate the correlation between vector dose and transduction efficiency with other pseudo-serotyped rAAV vectors, we injected mice with AAV1-EF1α-nlslacZ or AAV8-EF1α-nlslacZ via the portal vein at four different doses ranging from 5.0×10^{10} to 7.2×10^{12} vg/mouse, i.e., 5.0×10^{10}, 3.0×10^{11}, 1.8×10^{12} and 7.2×10^{12} vg/mouse ($n = 3$ to 6 per group). As a reference, we also injected six mice with 3.0×10^{11} vg of AAV2-EF1α-nlslacZ. Control mice were injected with the excipient (PBS–5% sorbitol) only ($n = 3$). Six weeks after vector injection, we harvested the liver samples and determined the transduction efficiency by counting β-galactosidase-expressing hepatocytes, measuring β-galactosidase antigen levels by enzyme-linked immunosorbent assay and quantifying the double-stranded vector genome copy numbers in the liver by Southern blot. The results are summarized in Table 1 and Fig. 1, and representative microscopic pictures are shown in Fig. 2.

As demonstrated, all the hepatocytes were permissive to stable transduction with the rAAV8 vector, reaching ≈100% hepatocyte transduction at 7.2×10^{12} vg/mouse. β-Galactosidase-positive cells with a small nucleus were occasionally found in the rAAV8-transduced liver (Fig. 2B). X-Gal/Kupffer cell double staining revealed no transduction in Kupffer cells (Fig. 2D). The origin of β-galactosidase-positive small nuclei could not be determined conclusively. These might be portions of hepatocyte nuclei or represent rAAV8-transduced nonparenchymal cells besides Kupffer cells. The number of hepatocytes transduced with the rAAV1 vector was 24% at a dose of 7.2×10^{12} vg/mouse. Since injection of a vector dose higher than 10^{13}

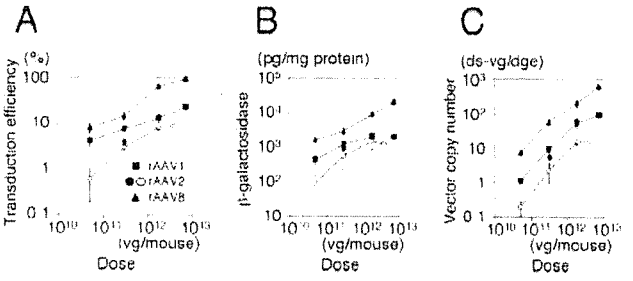

FIG. 1. Vector dose-response profiles in AAV1-, AAV2-, and AAV8-EF1α-nlslacZ-transduced mouse livers. The percentage of transduced hepatocytes in the livers (A), total β-galactosidase antigen levels (B), and number of double-stranded vector genomes per diploid genomic equivalent (ds-vg/dge) (C) are shown as a function of injected vector doses. Solid markers represent the values obtained from the present study. The dose-response profiles in AAV2-EF1α-nlslacZ-mediated liver transduction were obtained from our previous study (39) for comparison and are depicted with open circles. Values are means ± standard deviation.

vg/mouse was not feasible, it was not possible to determine the maximum number of hepatocytes permissive to stable rAAV1 transduction. Nonetheless, the results suggest that all the hepatocytes can process incoming single-stranded rAAV vector genomes into transgene-expressible double-stranded genomes without extrinsic assistance to augment transduction, such as providing adenovirus helper functions (11, 12), genotoxic treatment (1, 2), or forced biochemical modification of single-stranded DNA binding proteins (43-45, 61).

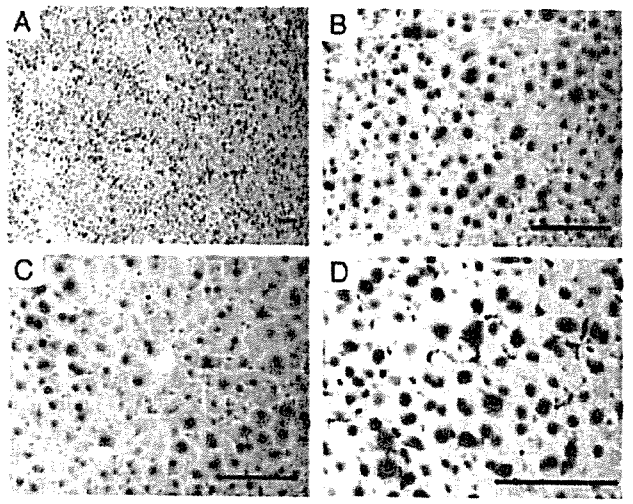

FIG. 2. Liver transduction with 7.2×10^{12} vg of AAV8-EF1α-nlslacZ delivered via the portal vein. The liver was harvested 6 weeks postinjection and stained with X-Gal and light hematoxylin. A representative result is shown (A and B). Virtually all hepatocytes were transduced with rAAV8 throughout the liver. The liver was stained heterogeneously with X-Gal, with central vein areas being less intense. (C) X-Gal-stained hepatocytes around a central vein area. Although gene expression near central veins was not as strong as in portal areas, most of the hepatocytes express the transgene. (D) X-Gal and F4/80 double staining. None of the Kupffer cells (brown) were transduced. Small nuclei positive for β-galactosidase are indicated with arrows in panels B and D. These might be portions of hepatocyte nuclei or represent rAAV8-transduced nonparenchymal cells besides Kupffer cells. Scale bars, 100 μm.

Dose-response profile with the rAAV8 vector did not change until all the hepatocytes were transduced. In rAAV2-mediated liver transduction, a proportional dose-response profile does not change at doses of less than 3.0×10^{11} vg/mouse, but the vector dose-response reaches saturation at higher doses (39). Likewise, our previous and present studies showed that the dose-response profile in rAAV1-mediated liver transduction changes between a low dose range (showing a disproportionately greater dose-response) and a high dose range (showing a blunted dose-response) (17) (Fig. 1B).

In the rAAV8-mediated liver transduction, log/log plots of the vector doses and the number of transduced hepatocytes (Fig. 1A) or the level of transgene expression (Fig. 1B) exhibited linearity throughout the given vector doses, with regression coefficients (r) of 0.945 (Fig. 1A) and 0.995 (Fig. 1B). The log y/log x slopes of the dose-response curves were 0.450 (Fig. 1A) and 0.585 (Fig. 1B). The log y/log x slope for a proportional dose-response should be ≈1.0. Therefore, neither the dose-response determined by measuring the number of transduced hepatocytes nor that determined by measuring the transgene protein product was directly proportional to various vector doses. The similar values of both slopes (both are around 0.5) imply that the total amount of transgene product and the number of transduced hepatocytes correlate with each other. Although the dose-response with rAAV8 was not proportional, both the number of transduced hepatocytes and transgene expression levels predictably increased with a constant factor of exp(≈0.5). In other words, when the AAV8-EF1α-nlslacZ vector is injected into mice at doses of 5.0×10^{10} vg/mouse or higher, an x-fold increase in the vector dose results in $x^{\sim 0.5}$-fold increase in the number of transduced hepatocytes and transgene expression until all the hepatocytes are transduced.

Total number of stably transduced double-stranded vector genomes in the liver increased in proportion to given vector doses irrespective of serotype. Next we determined double-stranded vector genome copy numbers per diploid genomic equivalent (ds-vg/dge) in the livers by Southern blot analysis. The results are summarized in Table 1 and Fig. 1C. In Fig. 1C, all vectors showed similar log y/log x slopes close to 1.0 (i.e., 0.775, 1.005, and 1.119 for rAAV8, rAAV1 and rAAV2, respectively) with a regression coefficient (r) of 0.999 in each case until the slopes of the dose-response curves started decreasing. This demonstrates that the total number of stably transduced double-stranded vector genomes in the liver increased proportionally irrespective of serotype until the saturation dose was reached. Considering that each of the three serotypes display distinct dose-response profiles, it is conceivable that the quality or state but not the absolute quantity of the double-stranded vector genomes in hepatocytes determines the dose-response profiles.

Decreased specific activity of vector genomes in the liver was concordant with the emergence of vector genome concatemers. It is possible to deduce the specific activity of the double-stranded vector genomes by dividing β-galactosidase expression levels by vector genome copy numbers (Table 1). In rAAV1 or rAAV8-mediated liver transduction, vector genome specific activity decreased as the vector dose increased. This

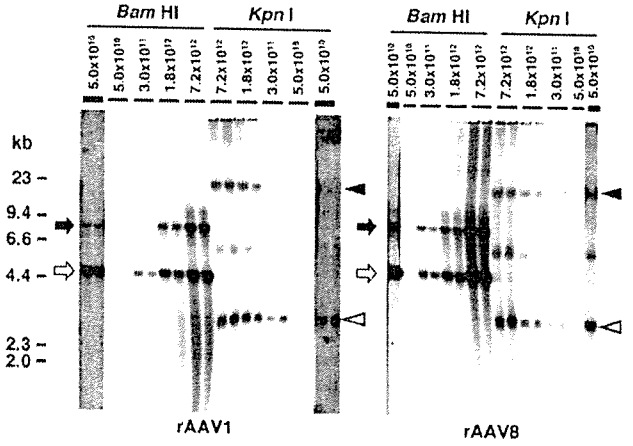

FIG. 3. Southern blot analysis of rAAV vector genomes in liver transduced with AAV1- or AAV8-EF1α-nlslacZ at various doses. The left and right panels show the results obtained with AAV1-EF1α-nlslacZ- and AAV8-EF1α-nlslacZ-injected mice. Total genomic DNA was extracted from the livers harvested 6 weeks postinjection and separated on 0.8% agarose gels following BamHI or KpnI digestion. BamHI cleaves the vector genome only once at nucleotide position 1362, while KpnI does not cut the 4,828-base genome. The vector genomes were detected with a 2.1-kb *lacZ* probe (nucleotide positions 1518 to 3639). Each lane represents an individual mouse. Injected vector doses (vg per mouse) are indicated above each lane. For the results obtained from the mice injected with 5.0×10^{10} vg/mouse, strips from overexposed blots are also shown to demonstrate the presence or absence of concatemers. They are indicated with thicker lines above the lanes. Open and solid arrows indicate head-to-tail and tail-to-tail molecules, respectively. Open and solid arrowheads indicate supercoiled double-stranded circular monomer vector genomes and concatemers, respectively. Head-to-tail molecules include both circular monomer genomes and concatemers, while tail-to-tail molecules represent concatemers exclusively. Therefore, the intensity of tail-to-tail molecules well correlates with the abundance of concatemers.

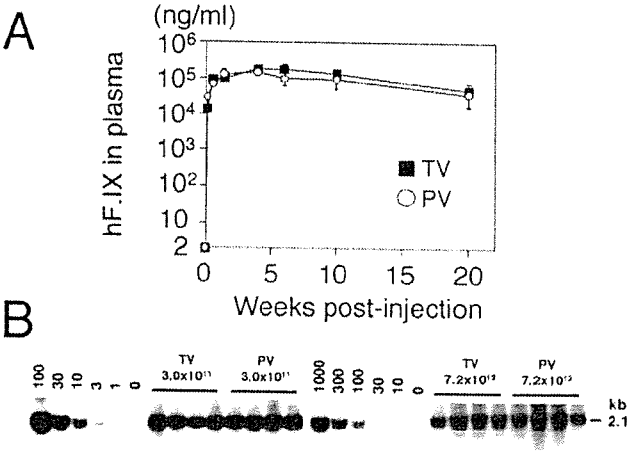

FIG. 4. Comparison of efficiency of rAAV8-mediated liver transduction between tail vein and portal vein injections. (A) Plasma human coagulation factor IX (hF.IX) levels after tail vein (TV) or portal vein (PV) injection of AAV8-hF.IX16 into male C57BL/6 mice. Robust human coagulation factor IX expression with no lag phase was observed with both routes. Expression peaked 4 weeks after injection, followed by a substantial (≈75%) decline. Vertical bars indicate standard deviations. (B) Vector genome copy numbers (ds-vg/dge) in livers transduced with AAV8-EF1α-nlslacZ via tail vein or portal vein injection at 3.0×10^{11} or 7.2×10^{12} vg/mouse. Total liver DNA was extracted 6 weeks postinjection, and 10 μg of DNA was analyzed by Southern blot with BglI digestion and a 2.1-kb *lacZ* probe (BglI-BglI fragment). The left and right blots were analyzed separately with a different series of vector copy number standards. The double-stranded vector copy number standards (0 to 100 and 0 to 1,000 ds-vg/dge) were prepared by adding the corresponding amount of plasmid, pAAV-EF1α-nlslacZ, to 10 μg of liver DNA extracted from a naïve mouse. Each lane represents an individual mouse. Routes of administration and vector doses are indicated above the lanes.

was also the case for rAAV2 vectors (39). The mechanism of this decreased genome specific activity is not yet clear but is likely related to the formation of less active double-stranded vector molecules, presumably concatemers (39). The present study, combined with the results from our previous study (39), showed that decreased vector genome specific activity is concordant with the emergence of concatemers. At the lowest dose, 5.0×10^{10} vg/mouse, the rAAV8 vector genomes formed substantial concatemers, while rAAV1 and rAAV2 formed exclusively circular monomers (Fig. 3) (39). The vector genome specific activities of rAAV1, rAAV2, and rAAV8 at this dose were 377, 489, and 223 (pg/mg of protein)/(ds-vg/dge), respectively, which is consistent with our presumption that concatemer formation decreases vector genome specific activity.

Comparison of tail (peripheral) vein and portal vein injection of rAAV8 vectors. Recently, Sarkar et al. reported that tail vein injection was as efficient as portal vein injection in the context of the canine coagulation factor VIII-expressing rAAV8 vector at a dose of 1.0×10^{11} vg/mouse (49). In our previous studies, we found that, with multiple serotypes, rAAV transduction was more efficient when delivered by the portal vein compared to the tail vein (17, 35). To further address this issue, we injected male C57BL/6 mice with 3.0×10^{11} vg of the rAAV8-hF.IX16 vector via the portal vein or the tail vein and monitored plasma human coagulation factor IX levels. Figure 4A summarizes the results. Both routes of injection resulted in rapid and robust expression of human coagulation factor IX in mouse plasma with no significant difference in transgene expression (Student's *t* test, $P = 0.28$, with 4-week time point values). Human coagulation factor IX expression peaked 4 weeks postinjection at levels of around 200 μg/ml, one log higher than that obtainable with the corresponding rAAV2 vector, AAV2-hF.IX16 (17, 39). However, transgene expression declined thereafter to levels of 40 to 50 μg/ml. Such a decline in human coagulation factor IX expression has not been observed with AAV2-hF.IX16. The mechanism of the decline is currently unknown.

Next, in order to determine the transduction efficiency of rAAV8 in the liver, we injected male C57BL/6 *rag-1* mice with two different doses of AAV8-EF1α-nlslacZ (3.0×10^{11} and 7.2×10^{12} vg/mouse) via two different routes (tail vein and portal vein, $n = 4$ each), and determined liver transduction efficiency 6 weeks postinjection through histochemical and molecular analyses. Control mice received excipient only. Serum samples were collected for measurement of ALT levels at days 1, 3, and 10 after injection. As summarized in Table 2, liver transduction efficiency was comparable between the two routes of injection at any vector dose (Student's *t* test, $P = 0.27$ and 0.47 for the doses of 3.0×10^{11} and 7.2×10^{12} vg/mouse, respectively), achieving ≈90% transduction efficiency with 7.2×10^{12} vg/

TABLE 2. Comparison of portal vein and tail vein injection of AAV8-EF1α-nlslacZ 6 weeks postinjection

Vector dose (vg/mouse)	Mean transduction efficiency (%) ± SD (*n*)	
	Portal vein	Tail vein
3.0×10^{11}	24.2 ± 13.1 (4)	15.5 ± 6.2 (4)
7.2×10^{12}	85.4 ± 7.3 (4)	89.1 ± 6.3 (4)
0 (excipient)	0.0 (2)	0.0 (2)

mouse. These results were similar but not identical to the transduction efficiency found in the dose-response study (Table 1). This was presumed to result from a lot-to-lot variation of the two vector preparations and/or the use of a different batch of animals.

Southern blot analysis of liver DNA to assess vector genome copy numbers in the liver also supported the histological observations (Fig. 4B). The average vector copy numbers determined by densitometric analysis were 37.6 ± 8.8 (tail vein, 3.0×10^{11} vg/mouse), 47.1 ± 6.0 (portal vein, 3.0×10^{11} vg/mouse), 815.6 ± 203.7 (tail vein, 7.2×10^{12} vg/mouse), and 1,044.3 ± 410.2 (portal vein, 7.2×10^{12} vg/mouse) (mean ± standard deviation). There was no statistical difference in vector genome copy numbers between tail vein and portal vein injections (Student's *t* test, $P = 0.12$ and 0.36 for 3.0×10^{11} and 7.2×10^{12} vg/mouse, respectively). Importantly, we did not observe any significant increase in the ALT levels at any time point (data not shown), suggesting that these vector doses did not cause liver damage. In addition, all the mice tolerated such a high dose well, and we did not find any histological evidence of cell damage or inflammation in the liver.

High-dose rAAV8 injection transduced multiple organs with considerable efficiency. The experimental results described above suggested that peripheral vein injection of the rAAV8 vector is a promising strategy that can safely yield ≈100% hepatocyte transduction. Although the results are pertinent to future gene therapy trials, we need to take into consideration that this strategy may increase the chance of vector spillover into nonhepatic tissues at these higher doses. To address this issue, we performed a tissue distribution study with mice injected via the tail vein or portal vein with two different doses (3.0×10^{11} and 7.2×10^{12} vg/mouse) of AAV8-EF1α-nlslacZ (four different combinations, as shown in Table 2). Six weeks postinjection, the brain, lung, heart, spleen, kidney, pancreas, testis, intestines, and skeletal muscle were examined in addition to the liver. Tissue distribution was assessed by both histological X-Gal staining of tissue sections and Southern blot analysis of vector genomes in the tissue DNA. We initially used the human EF1α enhancer-promoter-driven marker gene because it has been shown to be ubiquitously expressed in transgenic animals in a wide range of mouse cell types (18). Representative results of X-Gal staining of each tissue harvested from the mice injected with excipient only (control) and 7.2×10^{12} vg/mouse via the tail vein are shown in Fig. 5A and B.

The study revealed that, at 3.0×10^{11} vg/mouse, very few β-galactosidase-expressing transduced cells were observed outside the liver. However, at 7.2×10^{12} vg/mouse, multiple organs contained many β-galactosidase-expressing cells (Fig. 5A and B). In particular, the brain, heart, and smooth muscles of the intestinal wall were relatively well transduced. The lung and pancreas also contained a considerable number of positive cells. In addition, vascular smooth muscle cells in a variety of tissues were often found to be strongly positive (Fig. 5D). In the pancreas, most of the positive cells were acinar cells and found outside the Langerhans islets. There was no difference in the distribution between tail vein and portal vein injections (data not shown).

In the brain, immunohistochemical analyses demonstrated that both neurons and glial cells were transduced (Fig. 5C). The transduced cells were distributed throughout the brain, including the cerebral cortex, striatum, hippocampus, thalamus, and cerebellum. There were several small foci where transduced cells were clustered (Fig. 5Be). Such foci include the median eminence and arcuate nucleus of the hypothalamus and basolateral nucleus of the amygdala. Purkinje cells in the cerebellum were regionally well transduced (Fig. 5Bf), as previously reported by others using rAAV2 vectors (13, 20).

In the testis, β-galactosidase-positive cells were occasionally observed but restricted to cells residing in the interstitial space. None of the cells in the seminiferous tubules were positive for β-galactosidase activity.

Southern blot analysis of DNA extracted from these tissues revealed that double-stranded vector genomes were detected in all tissues analyzed at relatively high levels (Fig. 6). The average double-stranded vector copy numbers in each tissue were 19.6 ds-vg/dge in the heart, 19.0 ds-vg/dge in the skeletal muscle, 14.4 ds-vg/dge in the lung, 13.7 ds-vg/dge in the kidney, 7.6 ds-vg/dge in the testis, 5.1 ds-vg/dge in the intestine, 4.2 ds-vg/dge in the spleen, 2.7 ds-vg/dge in the brain, and 2.1 ds-vg/dge in the pancreas (from the highest to the lowest). It should be noted that even in the tissues with few positive cells, such as the spleen, testis, and skeletal muscle, double-stranded rAAV8 vector genomes were detected at levels comparable to those in the tissues with many β-galactosidase-expressing cells, suggesting that the extent of β-galactosidase expression does not necessarily correlate with the level of vector genome dissemination.

Peripheral injection of a rAAV8 vector transduced all the skeletal and heart muscles and a majority of pancreatic cells in the context of the cytomegalovirus promoter. To further address the discrepancy of the histological and Southern blot analyses in the context of the AAV8-EF1α-nlslacZ vector, we repeated the tissue distribution study with the AAV8-CMV-lacZ vector. We injected C57BL/6 *rag-1* male mice via the tail vein with the AAV8-CMV-lacZ vector at a dose of 3.0×10^{11} or 7.2×10^{12} vg/mouse ($n = 2$ each). Three weeks after vector injection, we analyzed various tissues by X-Gal staining. At a dose of 3.0×10^{11} vg/mouse, hepatocytes were transduced at levels comparable to that with AAV8-EF1α-nlslacZ. However, interestingly, the best-transduced organ was not the liver but the heart. A majority of cardiomyocytes were transduced with AAV8-CMV-lacZ at a dose of 3.0×10^{11} vg/mouse (Fig. 5E), although not many β-galactosidase-expressing positive cells were observed in other nonhepatic tissues, including skeletal muscle.

At a dose of 7.2×10^{12} vg/mouse, the whole liver was transduced (Fig. 5E). Amazingly, AAV8-CMV-lacZ transduced the heart and skeletal muscles with an extremely high efficiency at this dose. The entire heart muscle was transduced, and virtually all the myofibers in skeletal muscles were trans-

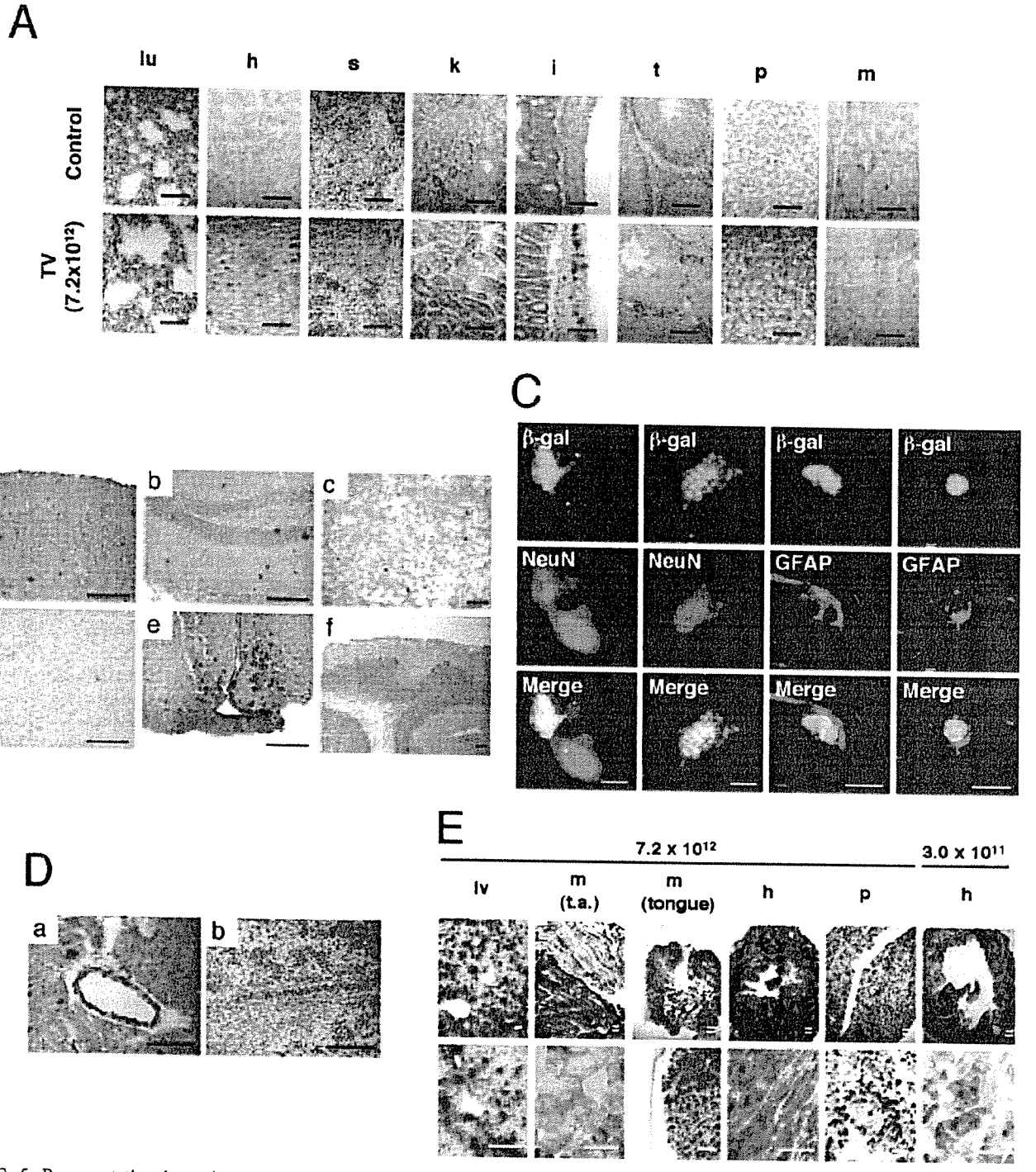

FIG. 5. Representative photomicrographs of sections of various mouse tissues 6 weeks after tail vein injection of AAV8-EF1α-nlslacZ at a dose of 7.2×10^{12} vg/mouse (A to D) or 3 weeks after tail vein injection of AAV8-CMV-lacZ at a dose of 3.0×10^{11} or 7.2×10^{12} vg/mouse (E). The sections were either X-Gal stained (A, B, D, and E) or stained with designated antibodies (C). (A) Tissue distribution of β-galactosidase-positive cells: lu, lung; h, heart; s, spleen; k, kidney; i, intestine; t, testis; p, pancreas; and m, skeletal muscle (quadriceps). The top row represents tissues from a mouse injected with excipient only, while the bottom row shows samples from vector-injected mice. (B) Brain transduction with rAAV8. (a) Cerebral cortex. Positive cells are scattered throughout the region. (b) Hippocampus. Positive cells are observed in both granule and pyramidal cell layers. (c) Striatum. (d) Amygdala. (e) Hypothalamus. β-Galactosidase-positive neurons and glial cells are clustered in the arcuate nucleus and median eminence. Some ependymal cells of the third ventricle are also positive. (f) Cerebellum. Purkinje cells are regionally well transduced. (C) Confocal microscopy to assess colocalization of β-galactosidase and either NeuN (a marker for neurons) or GFAP (a marker for astrocytes) to determine rAAV8-transduced cell types in the cerebral cortex of the brain. Both neurons and glial cells were transduced with rAAV8. Scale bars, 5 μm. (D) Transduction of vascular smooth muscle cells in the walls of a branch of the coronary artery (a) and a branch of the splenic artery (b). (E) Tissue distribution of β-galactosidase-positive cells in mice injected with AAV8-CMV-lacZ via the tail vein. The vector doses (vg/mouse) are indicated above the pictures. The section of the pancreas was also stained with anti-insulin antibody (brown cells). Scale bars (duplicated lines), 250 μm. lv, liver; t.a., tibialis anterior limb muscle. The tissues in panels A, B, D, and E were counterstained with nuclear fast red or light hematoxylin. Scale bars represent 100 μm unless otherwise noted.

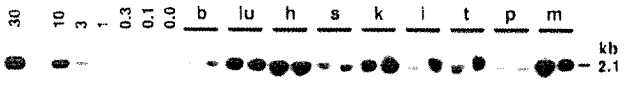

FIG. 6. Tissue distribution analysis by Southern blot. Various tissues were harvested from mice injected with 7.2×10^{12} vg of AAV8-EF1α-nlslacZ via the tail vein or the portal vein (one mouse each). Total genomic DNA was extracted from tissues, and 10 μg of each DNA was digested with BglI and separated on a 0.8% agarose gel. The vector genomes were detected with a 2.1-kb BglI-BglI *lacZ* probe. The double-stranded vector genome copy number standards (0 to 30 ds-vg/dge) were prepared as described in the legend to Fig. 4. Abbreviations: b, brain; lu, lung; h, heart; s, spleen; k, kidney; i, intestine; t, testis; p, pancreas; and m, skeletal muscle. In each set of tissues, the left and right lanes represent samples from mice injected via the tail vein and portal vein, respectively. For densitometric analysis, see the Results section.

duced (Fig. 5E). The whole-body X-Gal staining of a mouse injected intravenously with AAV8-CMV-lacZ revealed that all the skeletal muscles throughout the body, including the diaphragm, were completely transduced (data not shown). In addition, we observed substantial transduction of pancreatic acinar cells and islet cells (Fig. 5E).

Thus, the rAAV8 vector has strong tropism to the liver, but when high vector doses are systemically administered, the tropism becomes promiscuous, leading to undesirable transduction in nontarget tissues, particularly the heart, skeletal muscles, smooth muscles, pancreas, and brain. However, this opens up a new possibility that systemic administration of the rAAV8 vector can yield widespread transduction, with considerable efficiency, of a given target tissue.

DISCUSSION

The present study was conducted to investigate whether rAAV vectors of alternative serotypes can stably transduce all hepatocytes by administration of a high vector dose. To address this issue, we have chosen the rAAV1 and rAAV8 vectors and performed a dose-response study with a nuclear localizing LacZ-expressing vector. Both vectors have been shown to have liver transduction kinetics distinct from that of rAAV2 vectors (15, 17, 54). Although the rAAV1 vector failed to transduce all the hepatocytes due to a blunted dose-response at high vector doses, the present study clearly demonstrated that the dose-response profile of rAAV8 remained unchanged throughout a wide range of vector doses until all the hepatocytes were stably transduced at 7.2×10^{12} vg/mouse. Excluding the self-complementary vectors discussed below, this is the first report that a rAAV vector can yield ≈100% hepatocyte transduction with no obvious toxicity after a simple, noninvasive peripheral vein injection. In addition, we demonstrated that intravenous injection of the rAAV8 vector into mice could transduce entire skeletal muscles throughout the body, the entire heart muscle, and substantial numbers of pancreatic cells, smooth muscle cells, and brain cells.

Our knowledge about the mechanisms of rAAV transduction is still very limited. We have been investigating why rAAV2 vectors can stably transduce only a subset of hepatocytes. Impaired vector uptake in a subset of hepatocytes cannot explain this observation because vector genomes were found in most of the hepatocytes a day following vector administration (32). Therefore, blocks at the level of post-vector entry processing should contribute to the restricted liver transduction with rAAV2. Such barriers include endosomal processing and viral coat modification, which involves the ubiquitin/proteasome system (9, 19), cytoplasmic trafficking (48, 50), nuclear entry, uncoating (54), conversion from single-stranded to double-stranded vector genomes (11, 12, 38), processing of double-stranded vector genomes into transcriptionally active molecules via vector genome recombination (8, 36), and stable residence in the nuclear environment, which allows transgene expression. It is not easy to reconcile various observations with some conflicts from different laboratories at this time, but several recent observations or innovations have provided several important clues to this issue.

Recently, self-complementary or double-stranded rAAV vectors have been developed (13, 30, 31, 57). Self-complementary rAAV vectors possess half-sized hairpin-like double-stranded vector genomes. The important feature of this vector is that it skips the requirement for duplex DNA formation from single-stranded vector genomes, which is one of the fundamental limiting steps for rAAV vector transduction (11, 12). It has recently been shown that ≈90% of hepatocytes could be stably transduced when the self-complementary rAAV serotype 2 vector carrying a marker gene was injected into mouse livers (57). This suggests that release of vector genomes from viral virions occurs in most of the hepatocytes, and therefore the mechanisms for restricted liver transduction should be related to the inefficiency of duplex DNA formation from single-stranded vector genomes. However, and importantly, this does not necessarily exclude the possibility that factors upstream of duplex DNA formation may contribute to the inefficiency of liver transduction with rAAV2.

At least two models have been proposed to address the inefficient duplex DNA formation in rAAV2-mediated liver transduction. The first model involves cellular machinery that directly regulates duplex vector genome formation. Recently, Zhong et al. demonstrated that, in T-cell protein tyrosine phosphate transgenic mice and FKBP52-knockout mice, the rAAV2 vector transduced 12 to 16 times more hepatocytes than the wild-type counterparts (61). In these mouse models, phosphorylated forms of FKBP52, known to bind to the AAV inverted terminal repeat and block second-strand synthesis (43), are downregulated or deficient. From their observations, they claimed that impaired duplex DNA formation by second-strand synthesis (11, 12) precludes efficient transduction. The second model involves an upstream factor, i.e., the rate of capsid uncoating indirectly determines the efficiency of duplex DNA formation. In this model proposed by Thomas et al. (54), slower capsid uncoating of rAAV2 than of rAAV8 limits the formation of duplex DNA in hepatocytes through annealing of complementary plus and minus single-stranded rAAV2 genomes (38), resulting in inefficient liver transduction with rAAV2 vectors. At present, however, we do not have a clear answer that explains why stable liver transduction with rAAV2, but not rAAV8, is restricted to a fraction of hepatocytes.

Nonetheless, the present study demonstrated that all hepatocytes are capable of processing single-stranded rAAV2 genomes (delivered with AAV8 capsids) into duplex DNA. This implies that viral capsid proteins, and not cellular factors by